Sonar Transducer Reliability Improvement Program (STRIP) FY 82 First Quarter Progress Report

R. W. TIMME

Transducer Branch
Underwater Sound Reference Detachment
P.O. Box 8337
Orlando, Florida 32856

January 1, 1982

DTIC
ELECTE
MAR 1 8 1982

B

NAVAL RESEARCH LABORATORY
Washington, D.C.

82 03 18 254

REPORT DOCUMENTATION PAGE	READ INSTRUCTIONS BEFORE COMPLETING FORM
1. REPORT NUMBER 2 GOVT ACCESSION NO. 3 RECIPIENT'S CATALOG NUMBER NRL Memorandum Report 4724 AD-A112 172	
4. TITLE (and Subtitle) (U) Sonar Transducer Reliability Improvement Program (STRIP) FY82 First Quarter Progress Report	5. TYPE OF REPORT & PERIOD COVERED Interim report on a continuing problem
	6. PERFORMING ORG. REPORT NUMBER
7. AUTHOR(s) R.W. Timme	8. CONTRACT OR GRANT NUMBER(s)
9. PERFORMING ORGANIZATION NAME AND ADDRESS Underwater Sound Reference Detachment Naval Research Laboratory P.O. Box 8337, Orlando, FL 32856	10. PROGRAM ELEMENT, PROJECT, TASK AREA & WORK UNIT NUMBERS Program Element: 24281 NRL Work Unit: 59-0584
11. CONTROLLING OFFICE NAME AND ADDRESS Naval Sea Systems Command (SEA63X5-1) Washington, DC 20362	12. REPORT DATE 1 January 1982
	13. NUMBER OF PAGES 52
14. MONITORING AGENCY NAME & ADDRESS(if different from Controlling Office)	15. SECURITY CLASS. (of this report) Unclassified
	15a. DECLASSIFICATION DOWNGRADING SCHEDULE N/A

16. DISTRIBUTION STATEMENT (of this Report)

Approved for public release; distribution unlimited

17. DISTRIBUTION STATEMENT (of the abstract entered in Block 20, if different from Report)

18. SUPPLEMENTARY NOTES

The Sonar Transducer Reliability Improvement Program (STRIP) is sponsored by Naval Sea Systems Command (SEA63X5)

19. KEY WORDS (Continue on reverse side if necessary and identify by block number)

Transducers	Connectors	Environmental tests	Shielding
Corona	Noise & vibration	Plastics	Rubbers
Transducer fluids	Pressure release	O-rings	
Encapsulation	Material evaluation	Ceramics	
Cables	Water permeation	Metal matrix composites	

20. ABSTRACT (Continue on reverse side if necessary and identify by block number)

Progress was limited in the first quarter of FY82 due to the delay in funding which resulted from the lack of a national budget. Work progressed in only 6 of the 21 work units, and only then because of special funding situations.

TABLE OF CONTENTS

A

SONAR TRANSDUCER RELIABILITY IMPROVEMENT PROGRAM
FY82 FIRST QUARTER PROGRESS REPORT

1. INTRODUCTION

1.1. Program Overview

The primary purpose of this program is to develop Critical Item
Product Fabrication Specifications to support the acquisition of reliable,
cost-effective fleet sonar transducers. This program will provide the
technology base for the development of overall transducer design specifica-
tions through: the definition of extraneous noise criteria, the definition
of reliability and life prediction models, the analysis of failure modes,
the collection of a statistical data base, the characterization and
specification of materials, the development and application of new design
concept and diagnostic procedures, and the development/application of
methods and facilities for accelerated life testing and extraneous noise
T&E measurements.

The output of this program will consist of the specifications,
standards, and formal documentation for the materials, components, and
processes necessary for the design, test evaluation, and ultimate
procurement of reliable fleet transducers. These deliverables will define
the required chemical composition and mechanical properties of materials,
interpret gathered reliability data to define failure rates and mechanisms,
define assembly, quality control, and diagnostic procedures, and define
the required methods for the performance and lifetime evaluation of
transducers.

The program is organized into four major Task Areas, each of which
contains several Project Areas, and, in turn, each one of which will
contain several specific Work Units that will change each year in response
to milestones established by the acquisition requirements. The
organizational structure is shown in Fig. 1.1.

The FY82 Program Plan for STRIP has been described in detail in
Appendix A of NRL Memorandum Report 4615.[1] The specific work units and
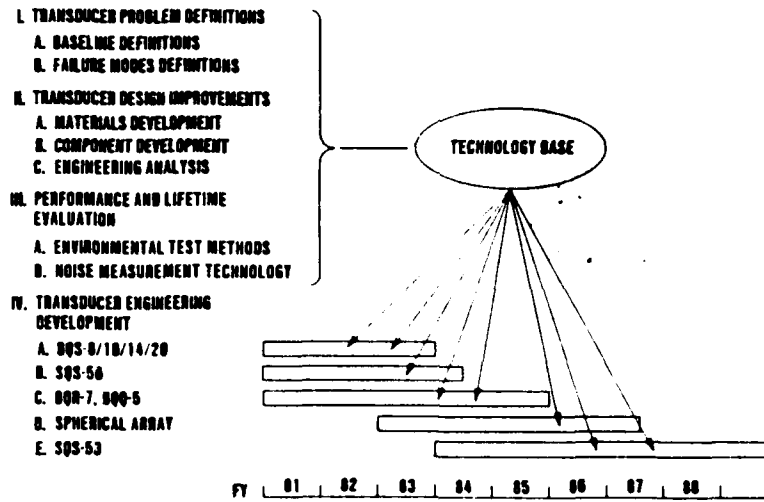their principal investigators for FY82 are given in Table 1.1.

1

I. TRANSDUCER PROBLEM DEFINITIONS
  A. BASELINE DEFINITIONS
  B. FAILURE MODES DEFINITIONS

II. TRANSDUCER DESIGN IMPROVEMENTS
  A. MATERIALS DEVELOPMENT
  B. COMPONENT DEVELOPMENT
  C. ENGINEERING ANALYSIS

III. PERFORMANCE AND LIFETIME EVALUATION
  A. ENVIRONMENTAL TEST METHODS
  B. NOISE MEASUREMENT TECHNOLOGY

IV. TRANSDUCER ENGINEERING DEVELOPMENT
  A. SQS-8/18/14/28
  B. SQS-56
  C. BQR-7, SQQ-5
  D. SPHERICAL ARRAY
  E. SQS-53

TECHNOLOGY BASE

FY 81 82 83 84 85 86 87 88

Fig. 1.1 – Sonar Transducer Reliability Improvement Program

Table 1.1 – STRIP FY82 Work Effort

	WORK UNITS	PRINCIPAL INVESTIGATORS	
I.A.1.	Noise Criteria and Standards	NOSC	C.I. Bohman
I.A.2.	Identification of Noise Characteristics	NWSC	T.J. Laughlin
I.A.3.	Noise Data Analysis and Acquisition	DTNSRDC	G.M. Jebsen
I.A.4.	Lifetime Reliability Definitions	TRI	R.L. Smith
I.B.1.	Failure Modes from Water and CUALT Analysis	TRI	D.D. Barrett
II.A.1.	Transducer Elastomers	NRL	C.M. Thompson
II.A.2.	Transducer Ceramics	NRL	A.C. Tims
II.A.3.	Alternative Materials	NRL	R.Y. Ting
II.B.1.	Unshielded Cables	Georgia Tech	H.W. Denny
II.B.2.	Cable Splices	TRI	D.E. Glowe
II.B.3.	Corona Control	NRL	L.P. Browder
II.B.4.	Ceramic Stack Joints	NOSC	I.C. Lockwood
II.B.5.	Acoustic Emission Applications	NUSC	T.J. Mapes
II.C.1.	Engineering Analysis	NRL	R.W. Timme
III.A.1.	Composite Unit Accelerated Life Testing	NOSC	J. Wong
III.B.1.	Measurement Methodology	NRL	A.L. Van Buren
III.B.2.	Experimental Measurement Correlation	NOSC	C.I. Bohman
III.B.3.	Measurement Correlation Models	BBN	N.C. Martin
IV.A.1.	SQS/SQR Product Fabrication Specification	NOSC	D.L. Carson
IV.B.1.	SQS-56 Product Fabrication Specification	NOSC	D.L. Carson
IV.C.1.	D1-276( ) Product Fabrication Specification	NWSC	J.A. Parks

1.2. SUMMARY OF PROGRESS

Progress was extremely limited in the first quarter of FY82 because of the delay in funding which resulted from the lack of a national budget. Work progressed in only six of the 21 work units, and only then because of special funding situations.

1.3. PLANS

The annual program review of STRIP which is normally held in March of each year will not be held in 1982 because of the limited progress resulting from the delayed funding. The program will restart as soon as possible after funds are distributed.

1.4. REPORT ORGANIZATION

The remaining sections of this quarterly report will discuss the objectives, progress, and plans for the specific tasks included in the STRIP.

2. WORK UNIT I.B.1 FAILURE MODES FROM WATER

P.H. Carr (?) *- Texas Research Institute, Inc.*

2.1. BACKGROUND

The state of water which enters a transducer and its effects once inside are continuing problems in the sonar community. Important questions are:

- What impurities come through rubber seals with water permeation?

- Where is the internal water, adsorbed or vapor?

- What temperatures or heat flows occur within transducers when the ambient temperature changes or the device is driven?

- What value is desiccant in a transducer?

- How can the lifetime of a transducer be accelerated?

2.2. OBJECTIVE

The objective is to determine the effects of water or water vapor on the performance and lifetime of sonar transducers and hydrophones. Specifically, the effects of the neoprene seals on the permeant (and vice versa) and the electronic changes caused by the permeant are to be investigated.

2.3. PROGRESS

2.3.1. Water Effects on Transducers

This phase of the work has been completed with the conclusion that TR-208A transducers and others of similar geometry and construction which have experienced degradation of free-field voltage sensitivity and transmitting current response because of aging and internal water saturation can be restored to their original performance by very thorough drying.

The problem, of course, is obtaining the very thorough drying. When the same drying procedure was applied to another water saturated transducer, the X-308, the performance was not restored to the original. In each case, the transducers were first aged in a 70°C oven with internal 90% RH and then dried by connecting to a closed air-circulating system consisting of a small air pump, a desiccant tube filled with type 4A molecular sieve and $Mg(C\ell O_4)_2$, and tygon tubing. It was found that the X-308 contained 6.7 g of water, but since the air volume was capable of holding only 0.034 g of water at 89% RH, then 99.5% of the water was adsorbed on internal surfaces or absorbed into parts such as corprene or printed circuit boards. This value is comparable to that for the TR-208A where 98.2% was adsorbed or absorbed. Because of much more surface area and a much more complicated inner structure for the X-308, the time for the drying cycle must be

extended to achieve the same degree of recovery of properties as for the TR-208A.

2.3.2. Water Permeation Through Elastomers

Long-term experiments are continuing with DI and saltwater as permeants through Burke Neoprene 5109. Experiments were begun at 20, 40, 60, and 80°C. However, anomalous data seem to be appearing at 80°C, such as lower permeation rates than the 60° samples. Also, some deposit is appearing on the outer surface of the high temperature samples. To prevent extreme bulging of the rubber in the 80° test, the complete assembly was preheated to the test temperature before it was sealed.

Preliminary data are given in Table 2.1 for the results to date. Data for the three temperatures given in Table 2.1 were used to generate an Arrhenius plot for the determination of the energy of activation, E_a, for permeation of fresh water through Burke 5109. This plot is shown in Fig. 2.1. The permeation constant, P, for 5109 has been determined by Dr. Corley Thompson (NRL-USRD) to be 25 ng-cm/cm^2-hr-torr at 20°C. This value roughly agrees with TRI's room temperature P of 21.9 ng-cm/cm^3-hr-torr. There are, however, discrepancies between NRL's and TRI's elevated temperature data. TRI's calculated E_a was 12.2 kcal mole^{-1} compared to NRL's value of about 1 kcal mole^{-1}.

Table 2.1 - Permeation Data on Burke 5109

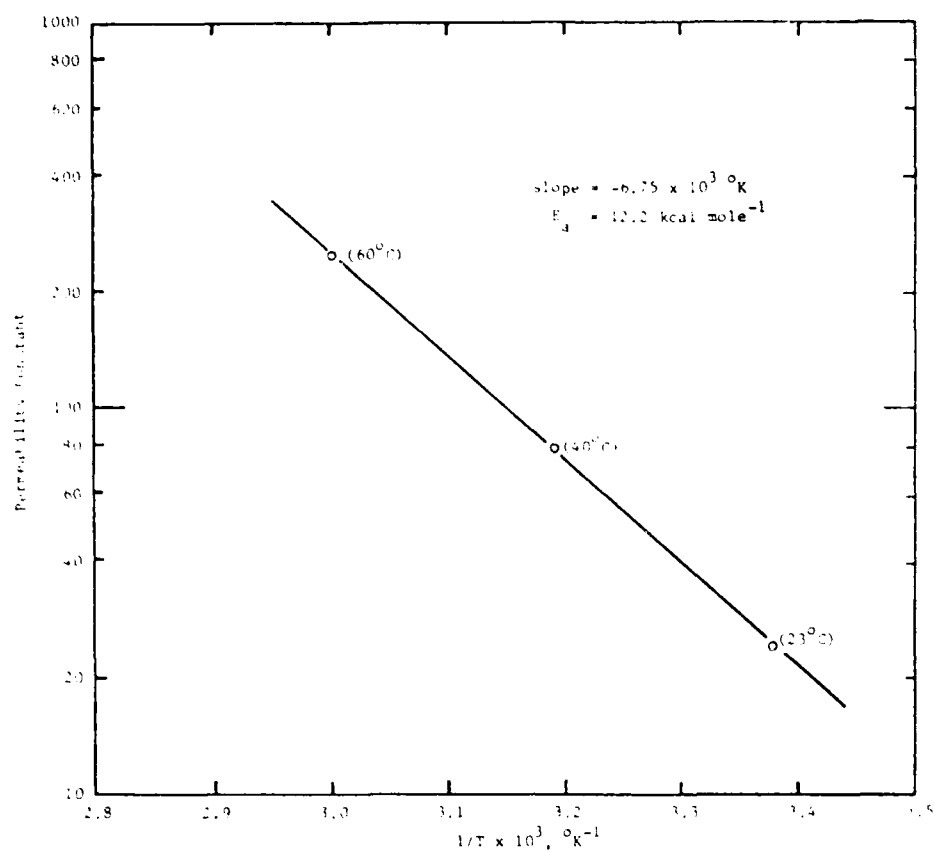| #	Condition	Permeation Rate, mg/cm^2/day	Total Flux, g	P, ng-cm/cm^2-hr-torr
1	23°/DI	0.050	0.059	21.9
2	23°/Salt	0.065	0.155	28.8
3	40°/DI	0.42	0.316	79.1
4	40°/Salt	0.41	0.465	78.7
5	60°/DI	3.67	2.435	256
6	60°/Salt	3.91	2.492	276
7	80°/DI	Restarted	---	---
8	80°/Salt	Restarted	---	---

Fig. 2.1 — Determination of the energy of activation
for permeation of deionized water through
Burke 5109 neoprene rubber

2.4. PLANS

Plans for the next quarter are to investigate how much water will an oil-filled transducer accept and where will it go.

3. WORK UNIT II.A.3 ALTERNATIVE MATERIALS: METAL MATRIX COMPOSITES

V. T. Abuquard? I - Process, II, Dr.

3.1. BACKGROUND

The main reason for considering metal matrix composites is to increase the bandwidth of the transducer. The bandwidth of the transducer is inversely related to the total energy stored in the vibrating system. If the stored energy is reduced in relation to the energy dissipated per cycle than the bandwidth will be increased. There is energy stored in the head, the ceramic, the tail, and some in the acoustic field. Of these, the head is unique because its velocity is the same velocity that flows into the load. So, in addition to the head being located where the velocity is maximum, that velocity cannot be reduced without reducing the energy radiated. Therefore, the only way to minimize its stored energy is to reduce its mass. This mass reduction is what the metal matrix composite material is expected to provide.

3.2. OBJECTIVE

The objective is to quantitatively compare and experimentally demonstrate the performance improvement possible with metal matrix composite materials for the head of longitudinal vibrator elements.

3.3. PROGRESS

Progress this quarter has been the establishment of an interface with the Navy activities, significant progress in the finite element analysis of vibrator heads, and ordering of silicon carbide particulate alum parts for the radiating heads.

Analysis of Head Vibrations

Finite Element Math Model of the Head. The ANSYS program is being used to calculate the head displacements. Support for this activity is being provided by Bruce Raymond of Control Data Corporation. The math model has been set up and check out is nearing completion. Selected trial cases at the extremes of the range of cases desired have been run and most of the computed results have been verified.

The model selected contains 90 nodes, 60 of which are shown in Fig. 3.1. The model is a figure of revolution with the left-hand line of nodes being the axis symmetry. For the calculations, sinusoidal drive is applied at nodes 12, 13, and 14. Stiffness elements corresponding to an estimated ceramic stack stiffness are connected between nodes 5 and 12 and between nodes 7 and 14. A stiffness corresponding to a stress bolt is connected between nodes 29 and 57. The stress bolt stiffness is assumed to be one-tenth of the ceramic stack stiffness.

Radiation mass loading is approximated by appropriately selected lumped masses at nodes 50 through 56. Radiation resistive loading is approximated by appropriately sized damping elements connected between nodes 50 through 56 and nodes 57 through 63.

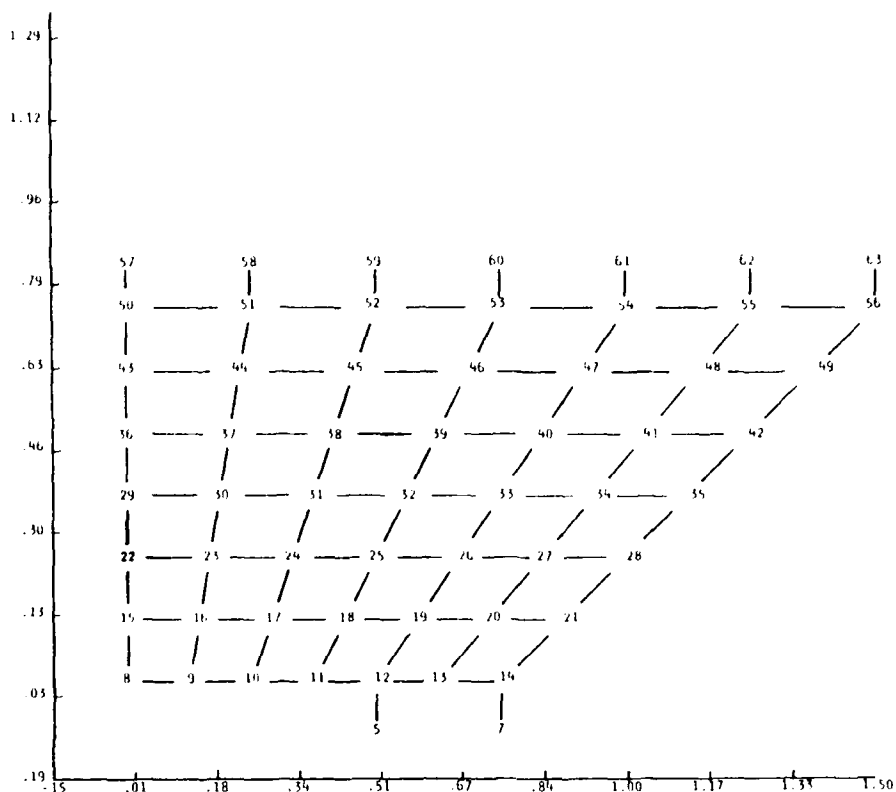Thirty degrees of freedom are used, sixteen of which are specified.

Fig. 3.1 - Finite Element Math Model

Computer Program Output Data. Three types of output data have been calculated and are being evaluated. These are: (1) calculation of the first 30 resonance frequencies; (2) calculation of the X and Y node displacement for frequencies from 1 to 25 kHz in 1 kHz steps, presented in tabular form; and (3) the same as #2 but presented in picture form.

To aid in the interpretation and evaluation of the results, a figure of merit has been defined and calculated. The figure of merit was desired to be the actual total volumetric displacement of the head, normalized to the desired displacement of the head. The desired displacement is defined as the area of the head times the displacement of the nodes of the back of the head where it is being driven with unit velocity (i.e., 1.000 ∠ 0° phase). The actual displacement of the head is calculated by summing the products of the face nodes times their appropriate areas. However, the face nodes are not all moving with the same phase relative to the drive velocity. To at least partially account for this condition, the velocity assigned to each of the face nodes in the figure of merit calculations is the amplitude times the cosine of its phase angle. This produces a snapshot of the head motion at some instant of time.

Material Procurement

Based upon preliminary results of the computer analysis, head sizes for the test specimens were selected and silicon carbide particulate parts were ordered from DWA. The parts are due to be delivered in early February. The thicknesses ordered are 2.54 cm and 1.90 cm. The parts, when received, will be machine-finished by a machine shop near DWA which is experienced in machining these parts. The material ordered is 35% volume of silicon carbide and has a Youngs modulus of about 1.38×10^5 MPa (20×10^6 psi), approximately double that of 6061 aluminum. The 35% VO material is about the highest silicon carbide content which can currently be made with a high confidence of good, consistent properties of the desired values.

3.5. PLANS

The following tasks are planned for the next quarter:

• Complete the math analysis.

• Build and test the models to support the analysis.

• Prepare the final project report.

4. WORK UNIT II.B.1 UNSHIELDED CABLES

R.W. Henry - Department of Electrical Engineering

4.1. BACKGROUND

Certain advantages such as better waterproofing, better water-blocking and lower cost would result from the use of underwater electrical cable without the internal shielding. The use of unshielded vs shielded cable has already been investigated from a mechanical strength viewpoint. The approach will now be to consider the electronics viewpoint of using unshielded or shielded cable on the outboard side of a submarine. Concerns are primarily centered upon electromagnetic interference and ground loops.

4.2. OBJECTIVE

The objective is to determine whether the use of unshielded cable in place of shielded cable, exterior to the hull of a submarine, will affect the electrical performance and reliability of sonar systems. Three tasks are associated with the accomplishment of this objective. These tasks are:

- Survey and analyze the installation of the DT-276 hydrophone of the BQR-7 and BQQ-5 systems on submarines to determine the electromagnetic interference (EMI) environment and the present practices of utilizing shielding on cables.

- Develop the theoretical modeling of shielded vs unshielded cables necessary and sufficient to predict the electrical performance and reliability of individual and arrays of DT-276 hydrophone in the EMI environment found exterior to the hull of a submarine.

- Devise and implement experimental procedures to verify the predictions from the second task.

4.3. PROGRESS

Work continued toward the determination of the current density on the exterior of a coaxial cylinder immersed in seawater. A coaxial model - an aluminum cylinder 15.2 cm in radius - was used to represent the submarine. The magnitude of the currents flowing in the seawater outside the outer conductor provide a measure of the field penetration of inside sources through the submarine hull. However, the dimensions of the submarine model and the resulting math model are such that the elements of the matrix vary greatly in their magnitude - the Bessel functions are on the order of 10^{14} and the Hankel functions are on the order of 10^{-17}. Because of such large differences, the matrix is ill-conditioned and yields a determinant that becomes numerically zero during the computerized calculations.

In order to validate the mathematical solution, it was decided to solve the equations for a smaller coax is seawater. The solution to the

matrix equation was carried out using standard computer techniques. The resulting current densities in the outer conductor and in the external seawater are shown Fig. 4.1. Note that the magnitude of the current density is fairly constant across the outer conductor, which, at a frequency of 400 Hz, is an expected result. The magnitude of the current density, however, drops by several orders of magnitude and continues to fall off steadily with increasing distance, again an expected result.
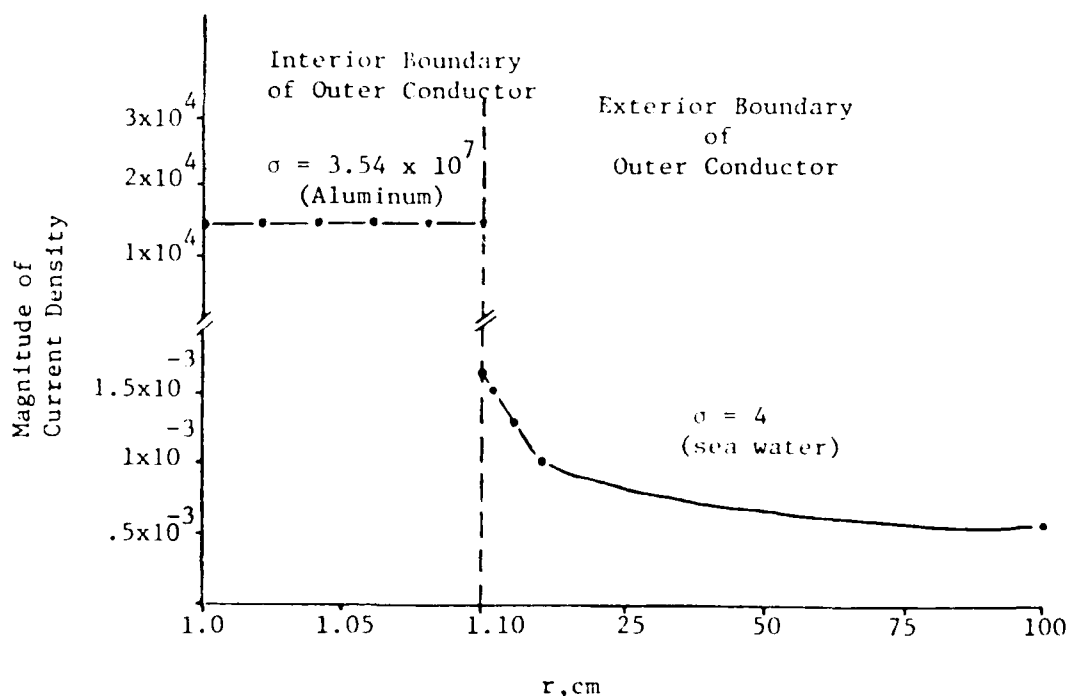

Fig. 4.1 – Current distribution in outer conductor and in exterior medium of coaxial cable immersed in seawater.

These results indicate that the matrix equation gives trustworthy current densities when the magnitude of the matrix elements are small enough to allow realistic calculations to be performed. The use of this method for a large-sized coaxial system is probably not practical, however, because the complex-valued Bessel function matrix elements are very sensitive to changes in the magnitude of their arguments. For example, a five-fold increase in magnitude can result in elements that will yield a matrix not useful for numerical calculation.

The investigation indicates that electromagnetic pick-up of external fields does not appear to be as serious as cable-to-cable coupling. Consequently, considerable emphasis is being directed at the analysis and measurement of cable-to-cable coupling in shielded and unshielded situations. The studies emphasize the actual cables (DSS-3 and DWU-3) in use rather than simulations. Although results produced by other types of cables should be relatable to DSS-3 and DSU-3, in the interest of

achieving maximum credibility from the program representative samples of
the two cable types will be needed. These cables have been requested f.om
the Naval Weapons Support Center.

Experimentally, preliminary cable coupling tests on a pair of parallel
wires over a ground plane were continued. These tests were carried out in
a small water tank environment as described in the two previous status
reports. At this time, attempts have been made to measure coupling with
the wires submerged in air only.

In order to increase the level of the coupling between the two wires,
the values of the load resistances were changed from those given previously
(Fig. 4.2). With these values, the coupled voltage, Vc, could be measured
easily without amplification and hence noise ceased to be a significant
problem. The driving voltage, Vs, was set at 19 Vpp and the frequency
range from 100 Hz to 100 kHz was spanned. The voltage, Vc, was measured
at each frequency and compared to the predicted voltages given by the
program XTALK. Figure 4.3 shows a comparison between the predicted
coupling and the measured coupling. At all frequencies, the measured
magnitude value is within 12.5% of the value predicted by the program XTALK.
For the phase, the maximum error is 6.5%. The average error for the
magnitude was 9.3% and for the phase the average error was 0.86%. These
data serve to validate the measurement technique.
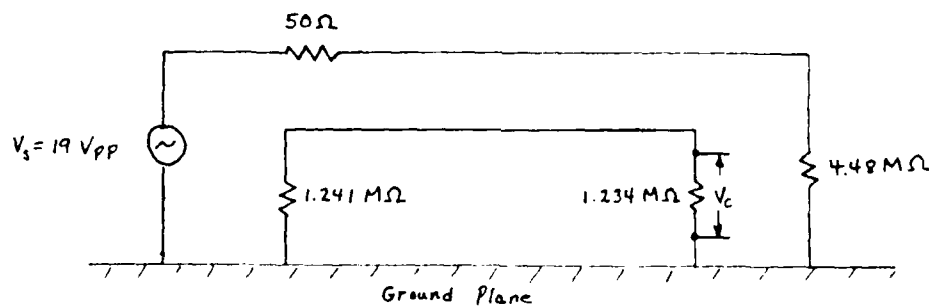
Fig. 4.2 - Experimental setup for coupling measurements
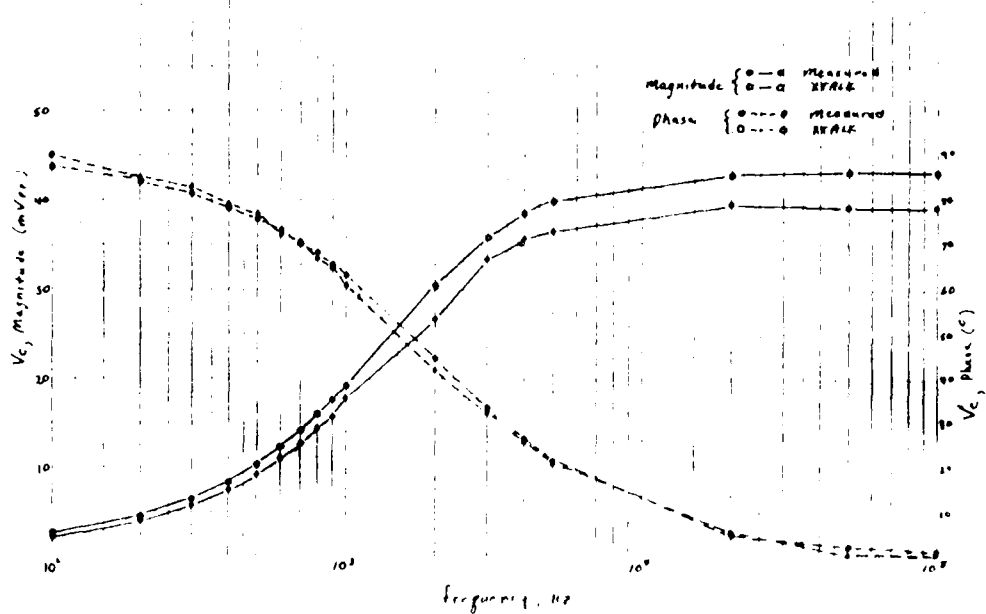
Fig. 4.3 – Magnitude and phase of induced voltage Vc

The computer program XTALK can be modified to be useful in lossy media, such as fresh or saltwater, simply by replacing the real permittivity ε by the complex effective permittivity

$$\epsilon_{ff} = (1 - j \frac{\sigma}{\omega \epsilon_0 \epsilon_r}) \ ,$$

where ϵ_r is the relative dielectric constant of the medium, σ is the conductivity, ω is the radian frequency, and ϵ_0 is the free-space permittivity. The losses in the medium ($\sigma = 0$) can be included without violating the TEM mode assumption or the uniqueness of voltage and current definitions. The next planned steps are to perform these measurements in fresh and saltwater media.

4.4.   PLANS

Plans for the second quarter FY82 are to:

   • Perform cable-to-cable coupling measurement in
     air and water and analyze results.

16

5. WORK UNIT II.B.3 CORONA CONTROL

5.1. BACKGROUND

A small but significant percentage of transducer failures is due to breakdown of electrical insulating materials. A physical phenomenon that contributes to these failures is corona. It is not practical to test the completed transducer to measure the effects of corona on lifetime and reliability. Corona formation and retardation must be studied at the component or piece-part level to locate and inhibit the damaging effects. Transducer reliability may then be improved by control of design parameters and construction processes.

5.2. OBJECTIVES

The objectives of this work unit for FY82 are:

- Study corona inception voltage characteristics of various electrode and material assemblies as used in transducers, including wiring, wire insulation, foil electrodes, and foil solder tab coatings.

- Provide recommendations, as required, for specific transducer improvements to avoid corona and for corona testing that will improve reliability.

- Prepare a handbook on transducer corona abatement and control that can be used to prepare transducer procurement specifications.

5.3. PROGRESS

5.3.1. Voltage endurance tests were performed on PZT ceramics with the insulating surfaces coated by Conap type CE-1171 material. Earlier tests had pointed to this material for further evaluation. The voltage endurance function obtained from these tests showed a lower average voltage breakdown than the results for other coating materials tested.[1] It also revealed a trend toward early breakdown. Other observations were that the cured material was hard and fractured easily. These findings do not commend Conap CE-1171 for use as an insulating coating for transducer ceramic surfaces.

5.3.2. A general goal of the corona control effort for transducers is to maintain the corona inception voltage (CIV) safely above the working voltage. The compact form of transducers may not contain enough space to use overdesign methods that avoid corona. Therefore, the physical principles that affect corona formation need to be applied to the design to ensure that adequate space is provided to meet the corona requirements.

Corona can occur if air or gas is in the insulating structure. The voltage level at which corona begins is dependent on (1) gas type, (2) gas pressure and temperature, (3) gas gap thickness, (4) solid insulation

thickness and dielectric constant, and (3) electrode shape. A typical structure that develops corona is a hook-up wire with contact points between the solid insulation and ground as shown in Fig. 5.1. Corona does not occur at the point of insulation contact but at some nearby location where the applied voltage is sufficient to break down the gas gap. The shape of the hook-up wire provides a range of series gas gap thickness.

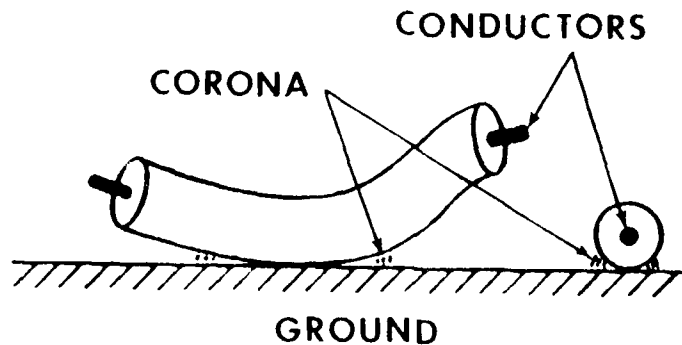Fig. 5.1 - Corona location for hook-up wires

Figure 5.2 shows a generalized series insulation structure where corona can form in the gas gap between the conductor and ground.
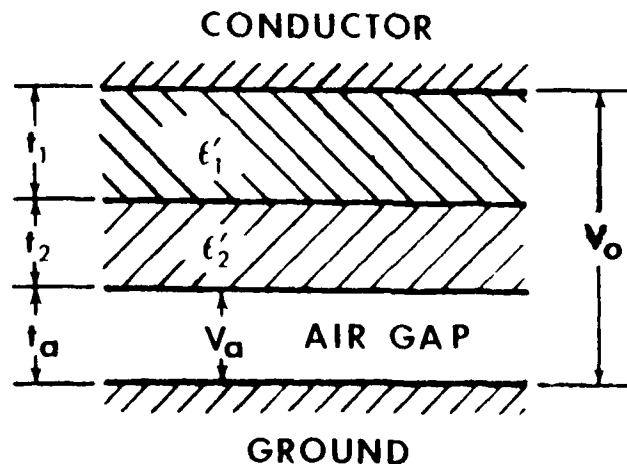

Fig. 5.2 - Series electrical insulation diagram

The distribution of the voltage across the structure is given by

$$V_o = \frac{V_g}{t_a}\left[t_a + \frac{t_1}{\epsilon_1'} + \frac{t_2}{\epsilon_2'} + \cdots\right], \qquad (5.1)$$

18

where V_g is the voltage across the gas gap of thickness t_g. Corona will occur in the gas gap when V_g exceeds the conditions of breakdown voltage V_b and gas gap distance given in Table 5.1. These values and Eq. (5.1) assume a uniform electric field for a specific gas at the applicable pressure and temperature. The data in Table 5.1 are for three different gases (air, nitrogen, and sulfur hexafluoride) that have been used in sonar transducers. The numbers given were obtained by interpolating the required points from curves measured by other investigators.[3] The data are considered correct for standard conditions of 20°C and 101.7 kPa (1 atm). For other conditions of gas temperature and pressure the value for t_g is modified using the equation

$$t_g' = t_g [(101.7 \; T')/(293 \; P')] , \qquad (5.2)$$

where t_g' is the new gas gap thickness, T' is the gas absolute temperature, and P' is the different gas pressure in kPa. Equation (5.2) is derived from the ideal gas law.

Table 5.1 – Breakdown voltages of 3 gases in a uniform electric field referred to 20°C and 101.3 kPa pressure.

GAS GAP DISTANCE (mm)	AIR V_b (kV-rms)	NITROGEN V_b (kV-rms)	SF_6 V_b (kV-rms)
0.0125	0.260	0.186	0.462
0.016	0.279	0.198	0.500
0.020	0.300	0.215	0.543
0.025	0.327	0.239	0.585
0.032	0.360	0.272	0.650
0.040	0.400	0.315	0.715
0.050	0.450	0.372	0.795
0.064	0.506	0.441	0.890
0.080	0.571	0.532	1.00
0.100	0.642	0.616	1.13
0.125	0.732	0.730	1.30
0.16	0.840	0.875	1.51
0.20	0.970	1.04	1.77
0.25	1.13	1.25	2.10
0.3	1.33	1.49	2.51
0.40	1.58	1.77	3.04
0.50	1.88	2.11	3.72
0.64	2.25	2.51	4.60
0.80	2.70	2.99	5.65
1.00	3.21	3.54	6.90

There is generally a range of gas gap thickness in any insulation assembly. If a series of calculations are made using Eq. (5.1) for one condition of solid insulating material (t_1/ϵ_1') and the air data from

Table 5.1, a curve similar to A in Fig. 5.3 is obtained. There is a minimum point on the curve that corresponds to the CIV for that condition. Other values for the quantity t_1/ϵ_1' in Eq. (5.1) will yield curves similar to B and C in Fig. 5.3. For any single condition of gas temperature and pressure, there is a minimum point on the curves dependent on the quantity $(t_1/\epsilon_1') + (t_2/\epsilon_2') + \cdots$ in Eq. (5.1). Curve D of Fig. 5.3 is a plot of the breakdown air data in Table 5.1.
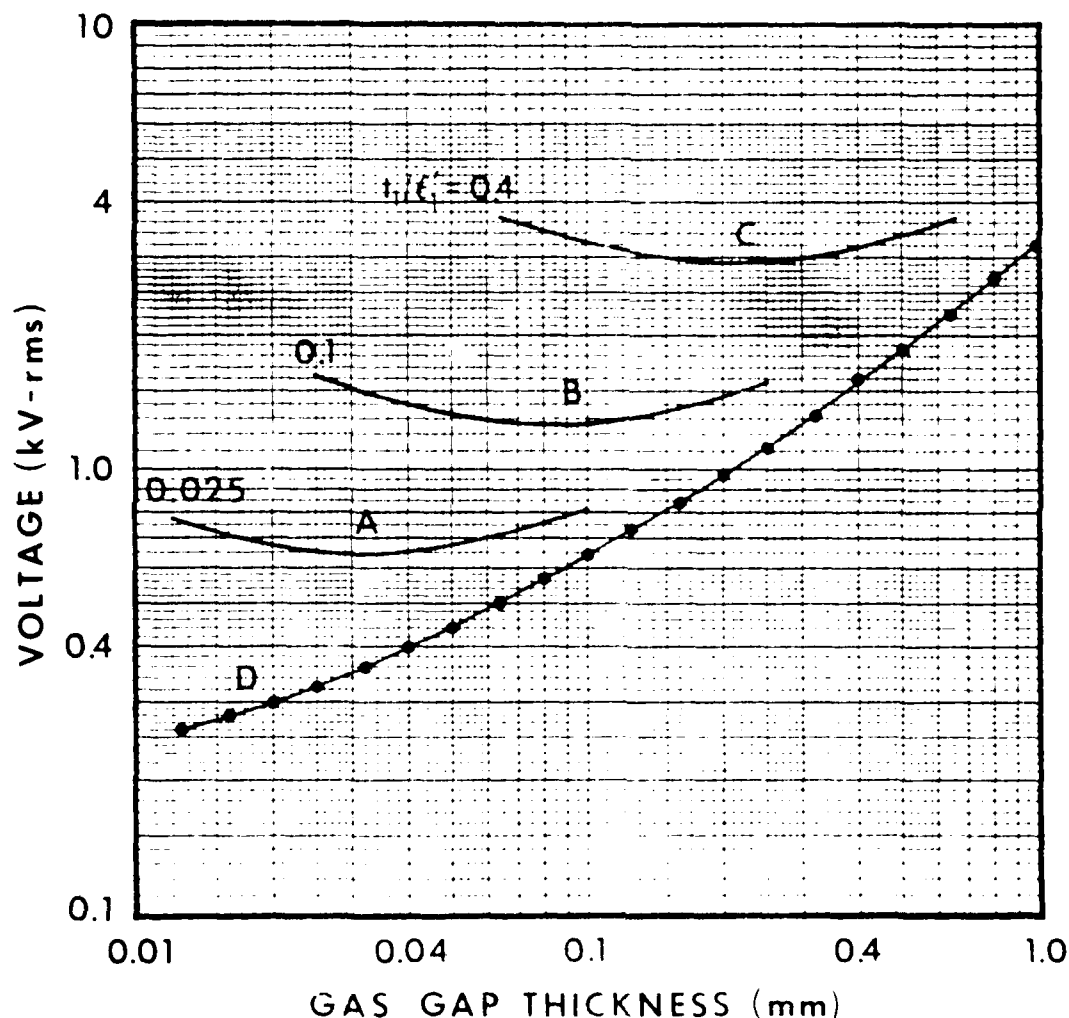
Fig. 5.3 Calculated curves for determining the minimum corona voltage

Figure 5.3 shows curves for minimum voltage points calculated using Eq. (5.1) with different values of the quantity t_1/ϵ_1'. Curves are given for each of the gas types included in Table 5.1 and also a curve for sulfur hexafluoride at the pressure of 1 atmosphere. These curves provide

a method to determine an appropriate corona inception voltage in many series insulation assemblies. The procedure is to calculate the quantity t_1/ϵ_1' for a single solid insulation system or $(t_1/\epsilon_1' + (t_2/\epsilon_2') + \cdots$ for multiple layers of insulation, enter that value on the abscissa of Fig. 5.4, and read the CIV on the ordinate corresponding to the point on the curve for the appropriate gas type.
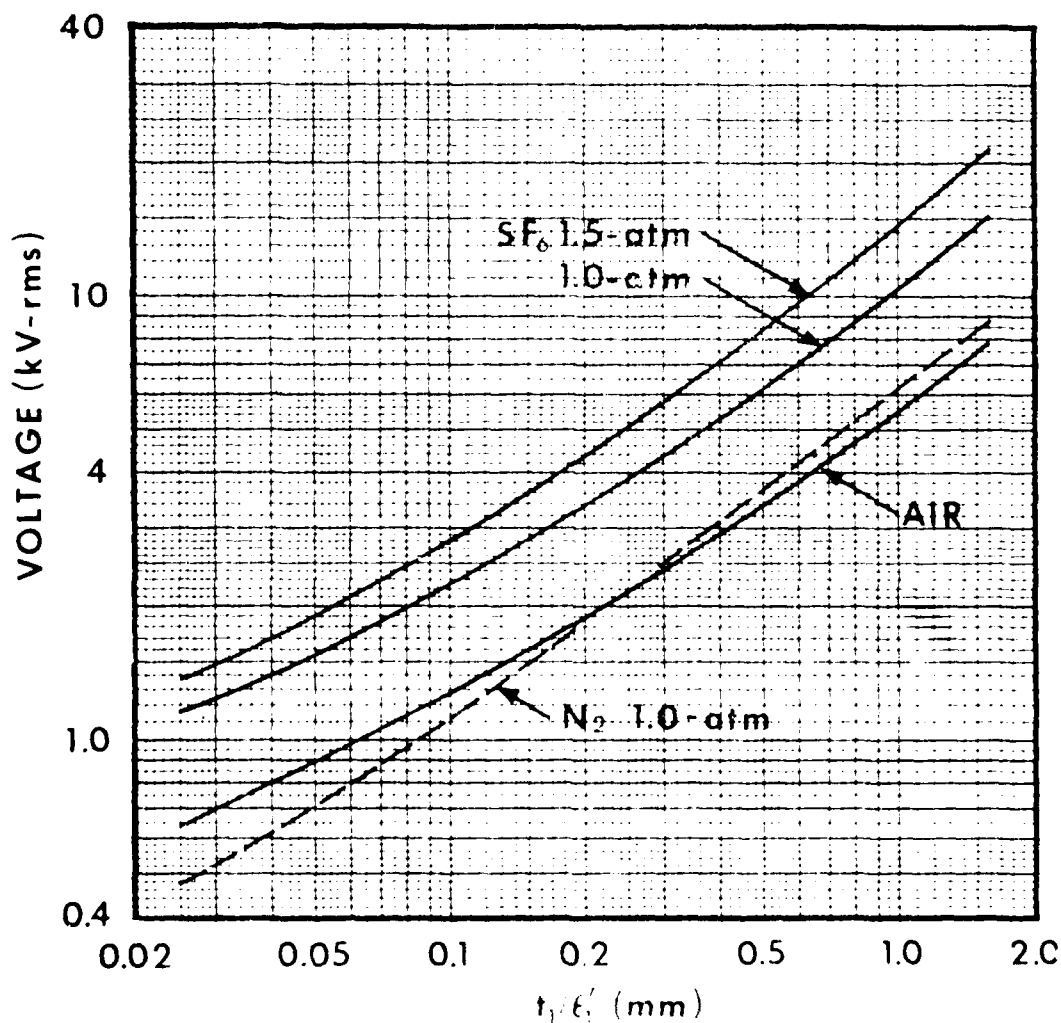
Fig. 5.4 — Calculated CIV curves for different series insulation thicknesses using air, nitrogen, and sulfur hexafluoride gases.

The curves of Fig. 5.4 only show trends in real situations. They are calculated from data for the uniform-field corona breakdown of the gases. If the electric field is divergent the CIV will occur at a lower voltage than shown. Preliminary tests in air field result that are 10-15% lower than the expected values. These differences in truth the corona range

from nearly uniform to a medium amount of divergence. More experimental
work is needed to determine the magnitude of this decrease of CIV with
divergent electric fields in air and the other gases.

The curves of Fig. 5.4 are experimentally verified when applied to
transducer ceramic that is fractured. Assume the ceramic thickness t_1 is
12.7 mm (0.5 in.) and its dielectric constant is 1000, then the ratio
calculated is 0.0127. An extrapolation of the air curve in Fig. 5.4 shows
that CIV is less than 0.5 kV. This is observed in corona tests on actual
ceramic and presents the possibility of using a corona test to detect
ceramic fractures after transducer shock tests.

5.3.3. A study was made to determine if one of the commonly used insulation
materials for hook-up wire was best for use in transducers.

- polyvinyl chloride
- polyethylene
- polypropylene
- nylon

- polytetrafluoroethylene (teflon)
- fluorinated ethylene
- polychlorotetrafluoroethylene
- polyvinylidine fluoride

A wide range of comparable characteristics were considered for the evalua-
tion. All of these materials have some dificiency that cause them to be
less than ideal. However, polyethylene and teflon were the materials
with the best composite score. The difficulty with polyethylene is its
high temperature limitation (+60°C) and with teflon is degradation in the
presence of corona. This investigation revealed no particular insulation
material that can be selected over the others.

Primary considerations for avoiding corona on hook-up wire are the
insulation thickness and dielectric constant as discussed in 5.3.2. For
instance, if corona is to be avoided on hook-up wire with teflon
insulation and is to be operated at 5 kV, it can be determined from
Fig. 5.4 that the insulation thickness should be at least 2 mm. If the
insulation is polyvinyl chloride, the thickness should be about 5 mm. Thus
a method to avoid corona on wiring is to use sleeving buildup of the
insulation, preferably using materials with a low dielectric constant.

5.4. PLANS

- Continue study of corona inception voltage effects using
  solid barrier insulation with various electrode shapes in
  three different gases.

- Study corona formation associated with foil electrode and
  solder joint geometry.

6. WORK UNIT II.C.1 ENGINEERING ANALYSIS

J. Hanish - NRL

6.1. BACKGROUND

The use of mathematical models for the prediction of performance of transducers and transducer components should be utilized. Many work units of STRIP aim at improving components such as ceramics, fluids, rubbers, etc. The effects of such improvements on transducers' performances need explicit evaluation. The initial approach will be to investigate the effect of the variation in ceramic properties on transducer performance using the TAC program and known production data on the ceramic. Later efforts will be to evaluate changes in other materials on transducer performance to determine the impact of "tight" vs "loose" specifications.

6.2. OBJECTIVES

The objective of this work unit is to develop and utilize mathematical models to predict transducer behavior, to make quantitative comparisons between predictions and evaluation results, to understand and resolve unexpected results, to provide guidance to R&D in materials, components, and noise, to provide contingency capability for future problem areas, and to provide engineering documentation interfacing the transducer procurements and systems applications with the R&D efforts.

6.3. PROGRESS

Although the physical principles of energy conversion of fleet transducers are relatively simple the do contain several complex mechanical components which make the prediction of their acoustic performance quite difficult. A successful approach, long in use among transducer designers, is to construct a mathematical model based on the use of idealized electrical and mechanical components. Realism is introduced by assigning to these components parameters whose numerical values are obtained by direct measurement on the prototype components themselves. The resultant mathematical model is translated into a computer program which then becomes available for predicting the effects of new design modifications or the effects of component failure. In essence, the computer model allows complex experiments to be conducted (on a transducer) in the laboratory without the presence of the physical object itself.

Of particular importance in this report is the proposal to explore changes in sonar transducer performance due to random variations in component properties, brought about either by relaxation of procurement specifications on an already existing component or by use of a new type replacement component whose manufacture is subject to small, uncontrollable variations.

The numerical experiment is of the Monte Carlo type. It comprises first, a determination of the probability distribution of the random variations in selected physical (or chemical) properties of the component. This distribution provides, in effect, a storehouse of random numbers from which an arbitrary selection can be made upon demand. The Monte Carlo

itself is a compilation of hundreds (or thousands) of performance predictions calculated successively by random number input made available from the random number storehouse.

Each component of a specific Navy transducer can thus be subjected to laboratory experimentation whenever its major properties are altered in any way. A chief reason for alteration is the overriding need to improve its reliability. Thus a quantitative measure of the balance between reliability and performance is obtained. This approach will first be applied to the TR-155 type transducer.

The Computer Model

Under Navy contract N00024-71-C-1290, project serial number S2239, task 1571, the General Electric Co. Heavy Military Electronic Systems, Syracuse, NY, prepared a "User's Manual to the Transducer Analysis Computer (TAC) Program" for the Naval Ship Systems Command (PMS0387), Washington, DC 20360. This manual was published in March 1972. In the TAC program the TR-155 is modeled as a longitudinal vibrator inside a mounting can, considered as an equivalent six-terminal (three-port) circuit, made up of a mechanical branch with two input and two output terminals, and a two-terminal (one-port) electrical branch coupled to the mechanical branch through an electromechanical transformer. The six-terminal circuit is decomposed into "black-boxes" connected to each other in series/parallel, with input-output terminals separately identified. It is shown in Fig. 1 of the user's manual. In the 31-transducer there is a simple large piezo-ceramic driver in the form of a hollow cylinder, 12.7-cm long, 10.2-cm diam, and 0.95-cm thick electroded on in the inner and outer surfaces. In the 33-transducer there are several hollow piezoceramic cylinders, electroded on the ends and cemented in echelon.

The method of analyzing the dynamic response of the TR-155 employed in the user's manual consists in treating each component "black-box" as having a mechanical input F_L, V_L (L = left) and a mechanical output F_R, V_R (R = right), and relating forces and velocities by use of impedance parameters. The mathematical model takes the form of a matrix equation. When, in addition, the component "black-box" has a one-connection electrical system as an input source, the parameters E, I are included in the matrix equation. Thus, in terms of impedance parameters Z_{ij} the general matrix relation which couples electrical to mechanical parameters becomes

$$\begin{pmatrix} F_L \\ F_R \\ E \end{pmatrix} = \begin{bmatrix} Z_{11} & Z_{12} & Z_{13} \\ Z_{21} & Z_{22} & Z_{23} \\ Z_{31} & Z_{32} & Z_{33} \end{bmatrix} \begin{pmatrix} V_L \\ V_R \\ I \end{pmatrix} \qquad (6.1)$$

Equation (6.1) has been selected by TAC to be the model of the piezoceramic cylinder and with E,I zero, also serves to model the components:

- an elastic rod
- an elastic cone

- a parallel mechanical impedance
- a parallel mechanical admittance

In essence TAC has been constructed in a direct, simple way in order to permit performance predictions to be made with minimum, but necessary, input. It accomplishes this by use of a group of easily accessible subroutines. A list of the most useful of these is presented below for ready reference:

SUBROUTINE CALL NAME	PERFORMANCE PARAMETER CALCULATED BY THE SUBROUTINE
LSW(12) = .TRUE	Electrical Admittance/Impedance
LSW(13) = .TRUE	Free-Field Radiation Loading
LSW(14) = .TRUE	Resonant Frequency
LSW(15) = .TRUE	Anti-Resonant Frequency
LSW(16) = .TRUE	Transmit and Receive Response
LSW(17) = .TRUE	Array Performance

These subroutines will be selected in subsequent reports to carry out a statistical evaluation by Monte Carlo methods of the effects of random variations in ceramic properties on electroacoustic performance of the TR-155.

Summary: Highlights of the TAC program have been briefly reviewed. More detailed analyses will be forthcoming in a second report. To use TAC one requires a number of inputs. However, it is emphasized that realistic inputs must come from measurements on prototype construction. This is discussed next.

Input Parameters and Their Relation to Experimental Measurements

The input to the TAC program consists of fixing the numerical values of many input parameters in the manner outlined in the user's manual. The procedure for making inputs is sufficiently complicated to warrant an extended review. However, to remain brief, the parameters are coupling coefficient, figure of merit, mechanical compliance, blocked capacity, electrical and mechanical loss factors, turns ratio, and mechanical Q.

In practice, the properties of the piezoceramics as measured by the transducer manufacturer are not directly insertable into the TAC. A conversion routine is used to transfer company-supplied data to the computer program itself.

TAC Application

The 31-mode piezoceramic cylinder that serves as a force/velocity generator in the TR-155 is shown in Fig. 6.1. In recent years the supplier has been obliged to furnish data cards for some 10% of a given procurement listing these properties:

- the stress-free electrical capacity (farads)
- the electrical tan δ_E
- the mechanical resonant frequency (kilohertz)
- the mechanical anti-resonant frequency (kilohertz)

Schematic representation of ceramic cylinder

We have obtained ... ... and issued by General
Electric under ... ... (... Data Item b40b) for
delivering ... ... In total, give
data on ... ... (Pa...) over a four-month
period. ... ... that ... the ... of the data presented on
these cards is ... , we have constructed histograms of the frequency of
occurrence of ... ... losses. The losses were determined by
first finding the ... and maximum value of a given ceramic property
(electric ... ... , frequency, etc.) arbitrarily dividing the
difference between ... values into ... equal classes. The
population in ... ... was then ... by a card routine. This histo-
gram construction ... of all data ... shown in Figs. ... through ...

Each histogram can be fitted by adjustment of floating numerical
constants to an empirical probability distribution. This fitting is
currently being ... ... A visual inspection, however, of the five
histograms (Figs. ... through ...) allows one to make the following
tentative choices of probability distributions:

TEST ... PROPERTY	... ... DISTRIBUTION
Free ... ... Capacity	... ...
...	... ...
Resonant	... ...
Anti-Resonant	... ...
Ratio of Anti-Resonant to Resonant Frequency	Two Population Gaussian (?)

These probability distributions, obtained by reasonable deduction, will be
compared with more accurately determined distributions in the next report.

```
FREOUENCY----------------------------------
  59  *       I                              *
  56  *       1                              *
  54  *       I                              *
  52  *       I                              *
  50  *       I                              *
  48  *       I                              *
  46  *       I                              *
  44  *       I                              *
  42  *       I                              *
  40  *       I                              *
  38  *       I                              *
  36  *       I  I                           *
  34  *       I  I  I                        *
  32  *       I  I  I                        *
  30  *       I  I  I                        *
  28  *       I  I  I                        *
  26  *       I  I  I                        *
  24  *       I  I  I                        *
  22  *       I  I  I  I                      *
  20  *       I  I  I  I                      *
  18  *       I  I  I  I                      *
  16  *       I  I  I  I                      *
  14  *       I  I  I  I                      *
  12  *       I  I  I  I                      *
  10  *    I  I  I  I  I  I                   *
   8  *    I  I  I  I  I  I                   *
   6  *    I  I  I  I  I  I                   *
   4  *    I  I  I  I  I  I                   *
   2  *    I  I  I  I  I  I                   *
-------------------------------------------
CLASS     2    4    6    8   10   12
```

Fig. 6.2 - Histogram of capacity C, constructed from data of Fig. 7; mean value = 28,741.8906 standard deviation = $0.52615 \cdot 10^2$

```
FREOUENCY----------------------------------
  51  *       I                              *
  49  *       I  I                           *
  47  *       I  I                           *
  45  *       I  I                           *
  43  *       I  I                           *
  41  *       I  I                           *
  39  *       I  I                           *
  37  *       I  I                           *
  35  *       I  I                           *
  33  *       I  I                           *
  31  *       I  I                           *
  29  *       I  I                           *
  27  *    I  I  I                           *
  25  *    I  I  I                           *
  23  *    I  I  I                           *
  21  *    I  I  I                           *
  19  *    I  I  I                           *
  17  *    I  I  I  I                        *
  15  *    I  I  I  I                        *
  13  *    I  I  I  I       I                *
  11  *    I  I  I  I       I                *
   9  *    I  I  I  I       I                *
   7  *    I  I  I  I  I  I  I                *
   5  *    I  I  I  I  I  I  I                *
   3  *    I  I  I  I  I  I  I                *
   1  *  I  I  I  I  I  I  I  I  I            *
-------------------------------------------
CLASS     2    4    6    8   10   12
```

Fig. 6.3 - Histogram of tan δ_E, constructed from data of Fig. 7; mean value = $16.48 \cdot 10^{-2}$ standard deviation = $0.33077 \cdot 10^1$

27

Fig. 6.6 – Histogram of F_x, constructed from data of Fig. 7;
mean value = 16,822.4883 Hz
standard deviation = 0.82052·10 Hz

Fig. 6.5 – Histogram of F_x, constructed from data of Fig. 7;
mean value = 18,791.8008 Hz
standard deviation = 0.11430·10 Hz

28

```
FREQUENCY-----------------------------
  42  *        I                      *
  41  *        I                      *
  40  *        I                      *
  39  *        I                      *
  38  *        I                      *
  37  *        I                      *
  36  *        I                      *
  35  *        I        I             *
  34  *        I        I             *
  33  *        I        I             *
  32  *        I        I             *
  31  *        I        I             *
  30  *        I        I             *
  29  *        I        I             *
  28  *     I  I        I             *
  27  *     I  I        I             *
  26  *     I  I        I             *
  25  *     I  I        I             *
  24  *     I  I        I             *
  23  *     I  I   I I  I             *
  22  *     I  I   I I  I             *
  21  *     I  I I I I  I             *
  20  *     I  I I I I  I             *
  19  *     I  I I I I  I             *
  18  *     I  I I I I  I             *
  17  *     I  I I I I  I             *
  16  *     I  I I I I  I             *
  15  *     I  I I I I  I             *
  14  *     I  I I I I  I             *
  13  *     I  I I I I I I            *
  12  *     I  I I I I I I            *
  11  *     I  I I I I I I            *
  10  *     I  I I I I I I            *
   9  *   I I  I I I I I I            *
   8  *   I I  I I I I I I            *
   7  *   I I  I I I I I I            *
   6  *   I I  I I I I I I            *
   5  *   I I  I I I I I I            *
   4  *   I I  I I I I I I            *
   3  *   I I  I I I I I I I          *
   2  *   I I  I I I I I I            *
   1  *   I I  I I I I I I I          *
-----------------------------------------
CLASS     2    4    6   8  10  12
```
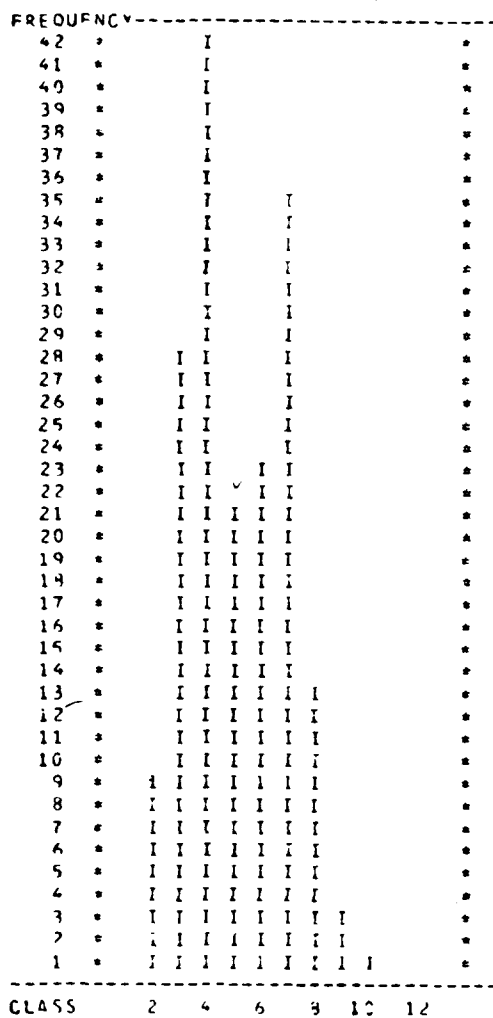
Fig. 6.6 – Histogram of F_n/F_m, constructed from data of Fig. 7; mean value = 1.1171 standard deviation = $0.10457 \cdot 10^{-1}$

6.4. PLANS

- Recognizing that the 175 point data base on ceramic properties falls somewhat short for a statistical analysis we shall seek to obtain at least 2000 data points.

- Once 2000 additional data points are obtained we will repeat the construction of histograms and their corresponding distributions by methods detailed above in this report.

- When all random parameters and their corresponding TAC inputs are in hand we plan to run a Monte Carlo experiment to determine the statistics of performance variation due to the random variations in ceramic properties as furnished by industrial suppliers.

- An interim report will then be issued.

29

7. WORK UNIT IV.B.1 SQS-56 Transducer Product Fabrication Specification

D.L. Carson - JHM

7.1. BACKGROUND

In the past the Navy has procured replacement sonar transducers using performance specifications which allow the successful bidder to radically change the transducer hardware design even in those cases where a very successful transducer had already been produced. This has often led to costly and time-consuming deficiencies and problems in the resulting hardware. The question has been asked "Why are sonar transducers different from other hardware; that is, why must we allow these changes once we have successfully produced a given sonar transducer?"

At present, the state-of-the-art is such that a stand-alone build-to-print specification is not likely to be successful, primarily because transducer performance is critically sensitive to electromechanical properties of the ceramic and current manufacturing techniques cannot economically ensure adequate consistency of these properties. Fortunately, it is possible to solve the problem being addressed without total adherence to the idealized goal. This is accomplished by relaxing the "build-to-print" requirements on certain components and processes in the transducer to allow for adjustments to compensate for ceramic variations. The problem is how to provide those design adjustment schemes in such a way that the contractor can reasonably be held responsible for unit performance while producing practical replicas of the proven transducer elements.

7.2. OBJECTIVES

The objectives of this task are to theoretically characterize and experimentally validate design adjustment schemes (DAS's) for possible inclusion in future SQS-56 Transducer Production Fabrication Specifications, which will produce practical near replica transducers on a production line basis. A secondary objective is to develop DAS data of more general applicability.

7.3. PROGRESS

An iterative approach is being applied to accomplish this task. Available theoretical models, experimental techniques, and minimum modifications of hardware are being utilized in the first iteration to produce results as fast as possible, and to determine where improvements are required. An effort is being made to have a good balance between theory and experiment. However, experiments of sufficient scope to provide statistically satisfying data are beyond the resources of this task. Therefore, every effort must be made to supplement the experimental evidence with data from production contracts.

At the initiation of the DAS herein described, a competitive buy of longitudinal vibrator transducer elements was anticipated for the SQS-56 sonar application. The critical item production specification represents a first effort to constrain the successful bidder to produce a "near replica" of a government selected and verified transducer element

31

design. This was accomplished ... certain dimensions and constraints
of the primary ... (such as
radiating head - all dimensions and tolerances; tail mass head fiberglass
washer - all dimensions and tolerances; piezoelectric rings - outside and
inside diameter dimensions and tolerances; stress rod - all dimensions and
tolerances; and the tail point mass), ... and constrains the
contractor to adjust ... The design
criterion specified ...
(defined as a frequency where the in-air conductance of the PSA is a relative
maximum) of ... configuration allows freedom
to select the length ... from the criterion. The
theoretical model, ... for the PSA shown in
Fig. 7.1 are taken ... The transducer
utilizing the PSA will ... as the reference element,
and denoted 56.980 (CM).

Fig. 7.1 - Nominal dimensions from front
surface of tail mass = 81.76 cm (4.13")

Due to time and money constraints in the original government design effort (resulting in the reference element), a theoretical radiation model for the array was not fully achieved. Therefore, one task in the first iteration has been to determine the problems for the array model, correct them, and to begin adapting the resulting array model as required for the present task. The lack of an adequate array model in the original design effort required that simplifying assumptions and constraints be placed on the class of permissible designs. This resulted in extensive reliance for design purposes on a single element in a rigid baffle predictive model. Much use has been made of the single-element model in the first iteration. It is believed that DAS trends deduced from single-element model predictions will be of great value to the task in their own right, as well as economical starting points for investigations involving the array model as it becomes available. In particular, all of the DAS observations reported herein are based on a model for a single element. The single-element model consists of a separate plane wave model for all of the components indicated in the primary assembly except for the radiating head. Thus far in a given transducer all ceramic rings have been assumed to be identical. Since it is known that the radiating head has significant flexing, this component was modeled using finite element theory with a corresponding acoustic radiation theory based on the half space Green's function.

Progress Based on Single-Element Model

In the original design effort resulting in the reference element the computer program was instructed to select the ceramic lengths to achieve the required F_m on the PSA, to select a parallel inductor (one component of the equivalent circuit for the autotransformer indicated in Fig. 7.2) which gives an in-water phase angle of $0°$ at 8 kHz, and to select the autotransformer turns ratio such as to make the minimum impedance in the transmit band equal to 160 ohms (changed to 195 ohms in the present analyses). The DAS's considered thus far are basically variations on these design criteria.

The component labeled "switching matrix" in Fig. 7.2 presents a short circuit in transmit but an open circuit in receive. Thus the autotransformer is not operative in the receive mode so that neither the turns ratio nor the inductance is available as part of a DAS for receive.

In order to proceed with the first-iteration analyses, it was necessary to establish, at least on a preliminary basis, the range of PZT-4 ceramic variations (i.e., the complex s_{33}, g_{33}, and polarization parameters). From discussions with ceramic manufacturers it became apparent that, although it was possible to obtain estimates of the extreme variations, no information was available as to the distributions. Moreover, there did not appear to be available any quantitative information on the correlation of parameter variations. A literature search revealed an article by Berlincourt that examines the variations of the ceramic parameters as functions of the thoroughness of poling. That work showed that as poling was varied, F_{33} and g_{33} varied in constant proportion, while s_{33} varied inversely with respect to the other two parameters. For the first-iteration analysis, the assumption that variations in the properties correspond to poling variations has been adopted. A maximum variation of $±7.5$ on each

parameter has been used. This value for the maximum variation has been adopted somewhat arbitrarily based on some measured data and the information provided by ceramic manufacturers.
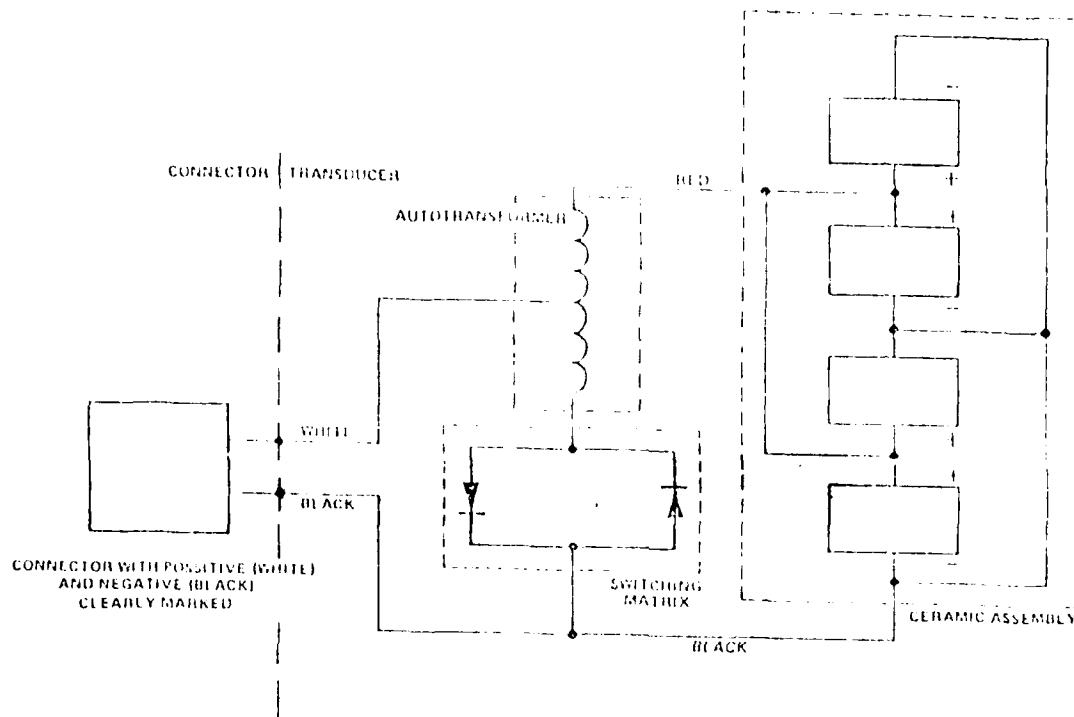

Fig. 7.2 — Typical transducer element schematic

Instead of considering only the length of the piezoelectric ceramic rings to adjust the PSA for variations in ceramic parameters, three different components of the PSA were considered independently as adjustments: ceramic ring lengths, head fiberglass washer length, and tail fiberglass washer length. For the range of ceramic parameter variations considered, it turns out that adjustments using any one of the three components considered (ceramic ring length, head fiberglass washer length, or tail fiberglass washer length) result in roughly the same single element performance. Some of the important differences are discussed below in conjunction with discussions of Figs. 7.3 through 7.6.

In the analyses that have been performed, the computer has been programmed to produce a plot that shows, as a function of frequency, each of the performance factors to be considered. In each of the computed examples shown (Figs. 7.3 through 7.6) seven curves are shown. Each curve corresponds to parameters that have been varied (both the real and imaginary parts) from those determined for the reference element by percentages shown in Table 7.1. Also shown are the symbols used to identify the corresponding curve. Table 7.2 lists the plots that are produced in each case. With reference to Table 7.2, Fig. 7.3 shows

examples of plot 1; Fig. 7.4 shows examples of plot 2; Fig. 7.5 shows examples of plot 3; and Fig. 7.6 shows examples of plot 4. In each figure the first three parts (for example, Fig. 7.3a, Fig. 7.3b, and Fig. 7.3c) represent the case where the head fiberglass washer is used to adjust the PSA, while the fourth part (Fig. 7.3d) the piezoelectric ceramic length adjustment is represented. The head fiberglass washer case was chosen because it gave one of the best results on the receive response (Fig. 7.5c) and otherwise illustrates the general trends. The ceramic stack length case is presented for comparison to illustrate differences among the cases.

As mentioned previously, the current product specification for the SQS-56 element calls for constraining F_m as a basis for the DAS. Using F_m as a design constraint (implemented by one or the other of the length adjustments discussed above) results in certain performance factors (such as input impedance magnitude) being almost identical (in the frequency band of interest) for the range of ceramic parameters considered, whereas certain others (such as input impedance phase angle) are deviating.

In an attempt to bring the remaining performance factors more into agreement, the use of F_n as a design constraint was tried. F_n is defined as the frequency where the in-air admittance of the PSA is a relative minimum. The F_n used is that of the reference element (8.70 kHz). It was found that use of F_n generally reverses the quantities which give agreement and which deviate. For example, using F_n, the impedance phase angles are almost overlays in the transmit band of interest whereas the impedance magnitudes vary. Comparison of Figs. 7.3a and 7.3c with Figs. 7.4a and 7.4c shows that matching F_m produced the best match of impedance magnitude in the transmit bands (indicated by ⋅⋅) while matching F_n produced the best match of impedance phase angle. Such trends occurred in general and this suggested the use of F_{AV} as the constraint, should one desire the best compromise DAS. The F_{AV} constraint was used for Figs. 7.3b and 7.4b. Therefore, the average frequency between F_m and F_n ($F_{AV} = (F_m + F_n)/2$) has been adopted as a third trial design constraint for the first-iteration analyses.

It is noteworthy that the SQS-56 system is more sensitive to input impedance phase angle than impedance magnitude due to the characteristics of the transmit power amplifiers. Thus, at least for input impedance considerations, the F_n match might be preferred over the F_m match as a DAS for the SQS-56 system.

Figure 7.6 indicates that matching F_m gives the best DAS for transmit voltage response. In fact, for the range of ceramic parameter variations considered (and the scale plotted) no differences are observable. On the other hand, none of the DAS's show drastic variations in transmit voltage response.

Recall (Fig. 7.2) that in receive, the autotransformer is disconnected from the circuit, and the receive band is from 3 to 10 kHz. Thus the only adjustments considered thus far in the receive mode are to the PSA. The least deviation in open-circuit receive response (the preamps have a very high impedance) observed thus far illustrated in Fig. 7.5c (matching F_n by adjusting the head fiberglass washer). The largest deviations over the frequency band are illustrated in Fig. 7.5d (matching F_n by adjusting ceramic length).
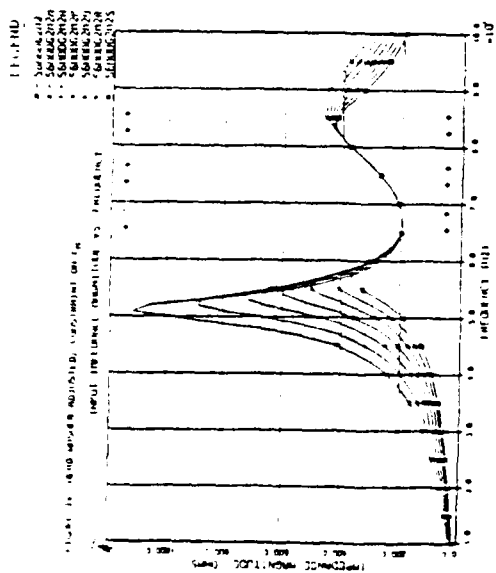
FIG. 7.3b – HEAD WASHER ADJUSTED, CONSTRAINT ON F_{RS}
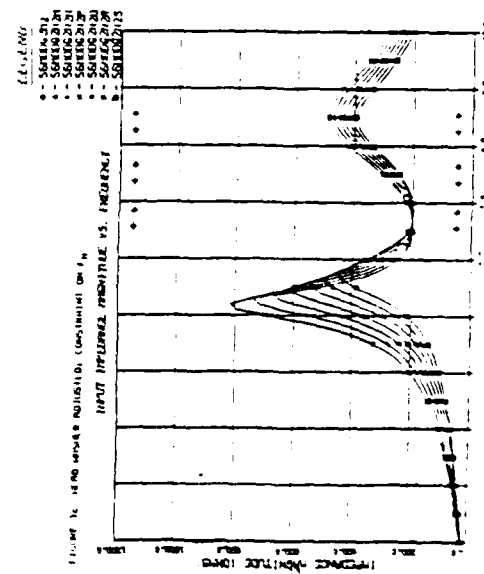
FIG. 7.3d – CERAMIC TENSION ADJUSTED, CONSTRAINT ON F_{R}

FIG. 7.3a – HEAD WASHER ADJUSTED, CONSTRAINT ON F_{M}

FIG. 7.3c – HEAD WASHER ADJUSTED, CONSTRAINT ON F_{N}

FIGURE 18 – HEAD WASHER ADJUSTED; CONSTRAINT ON F_{RV}
INPUT IMPEDANCE PHASE VS. FREQUENCY

FIG. – CERAMIC LENGTH ADJUSTED; CONSTRAINT ON F_{RV}
INPUT IMPEDANCE PHASE VS. FREQUENCY

FIGURE 19 – HEAD WASHER ADJUSTED; CONSTRAINT ON F_M
INPUT IMPEDANCE PHASE VS. FREQUENCY

FIGURE 19 – HEAD WASHER ADJUSTED; CONSTRAINT ON F_M
INPUT IMPEDANCE PHASE VS. FREQUENCY

FIGURE 8c - HEAD WASHER ADJUSTED; CONSTRAINT ON F_N

Fig. 7.bc - HEAD WASHER ADJUSTED; CONSTRAINT ON F_N

FIGURE 8d - FRAME LENGTH ADJUSTED, CONSTRAINT ON F_N

Fig. 7.bd - FRAME LENGTH ADJUSTED, CONSTRAINT ON F_N

FIGURE 8b - HEAD WASHER ADJUSTED; CONSTRAINT ON F_M

Fig. 7.ba - HEAD WASHER ADJUSTED; CONSTRAINT ON F_M

FIGURE 8a - HEAD WASHER ADJUSTED; CONSTRAINT ON F_{RV}

Fig. 7.b - HEAD WASHER ADJUSTED; CONSTRAINT ON F_{RV}

39
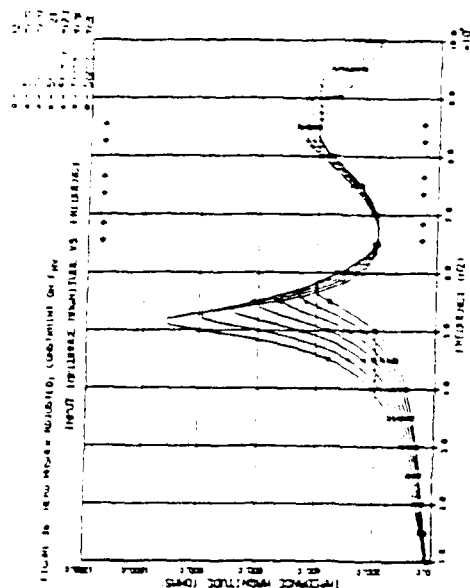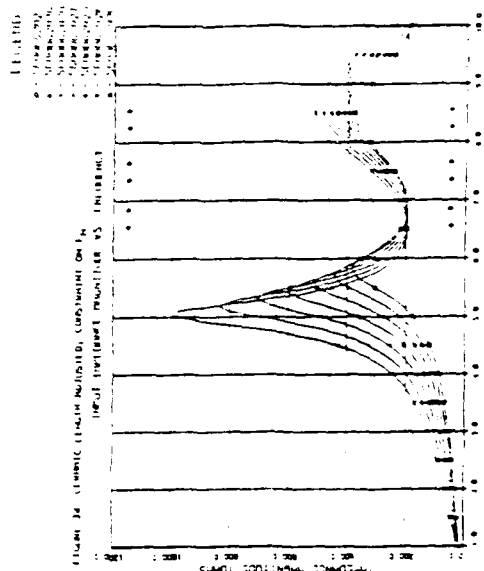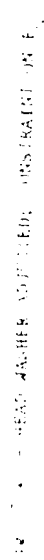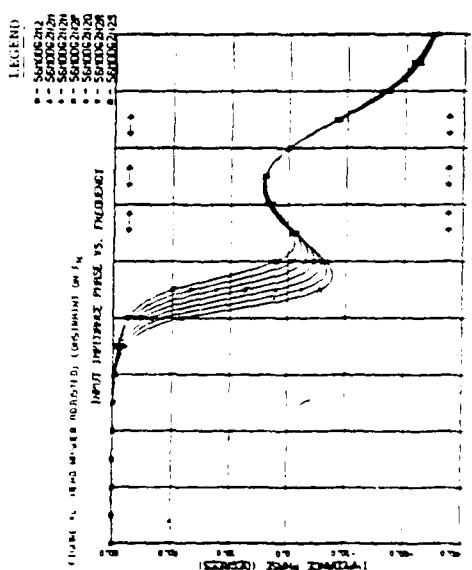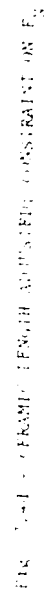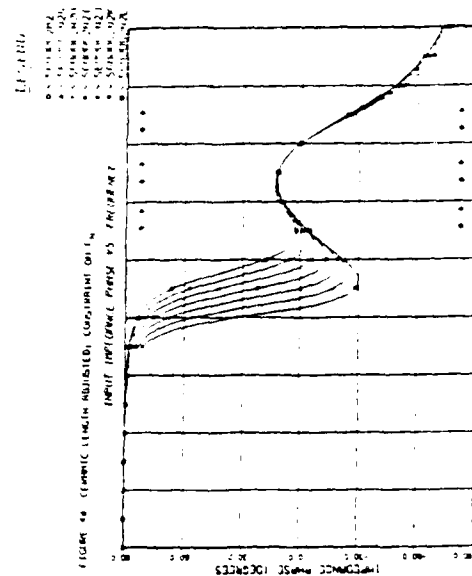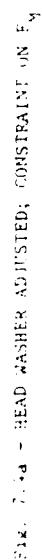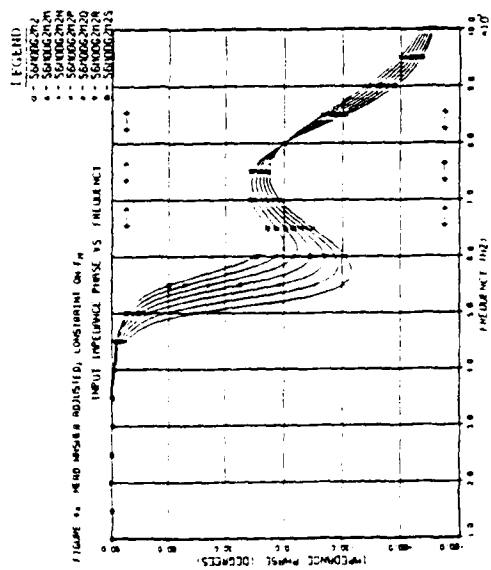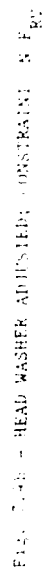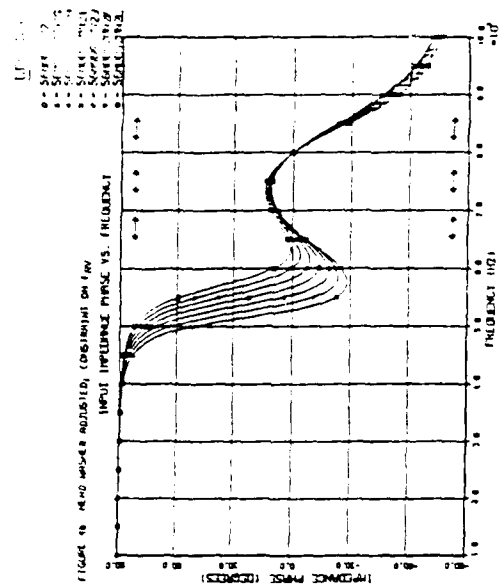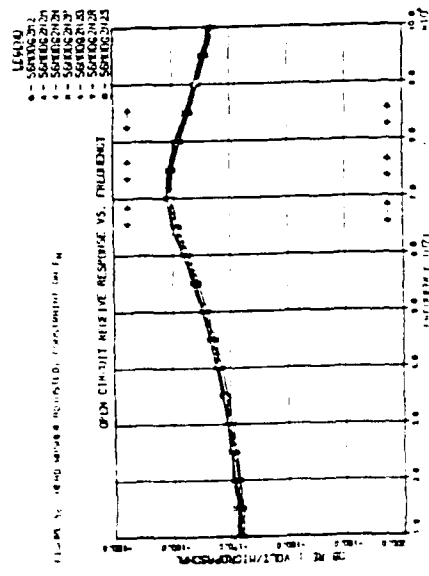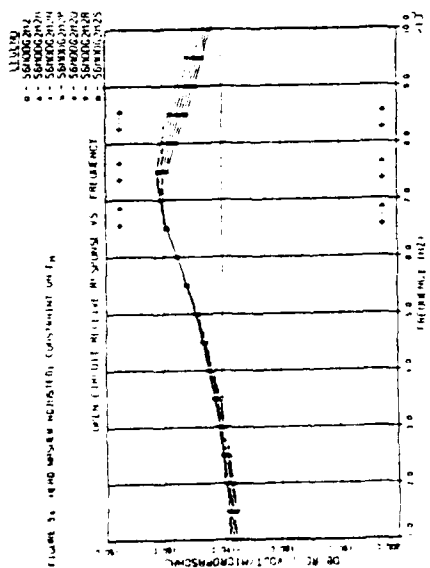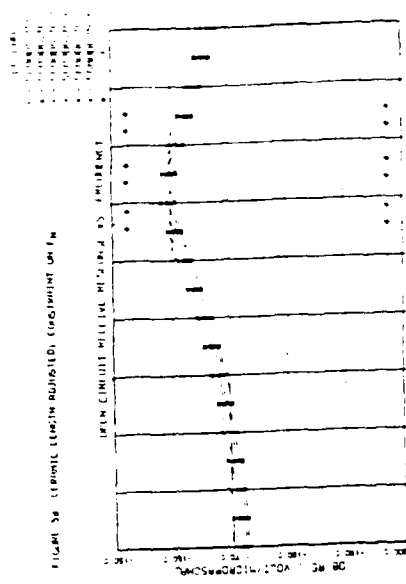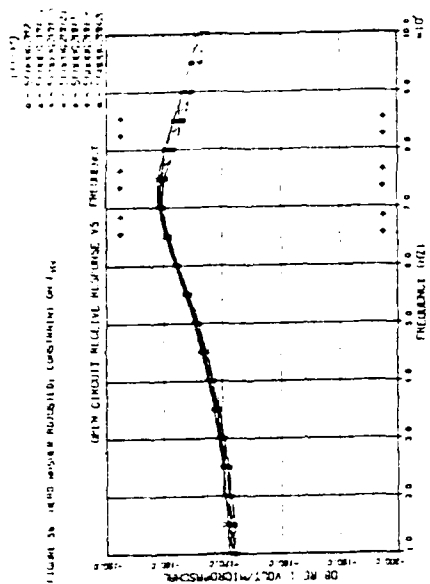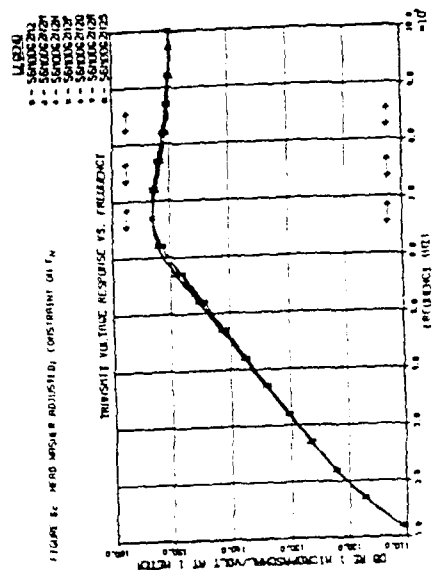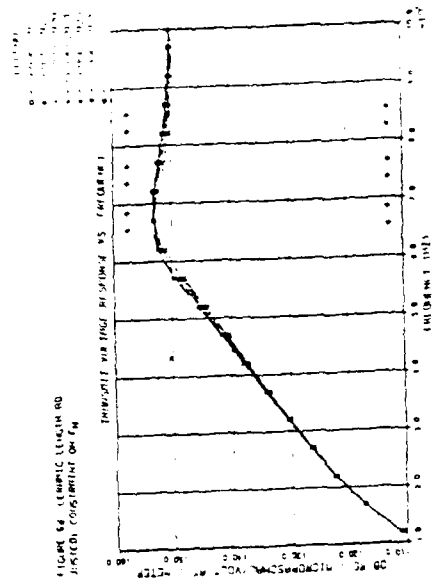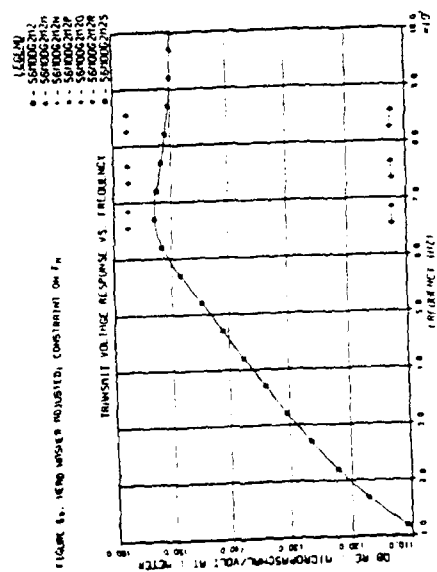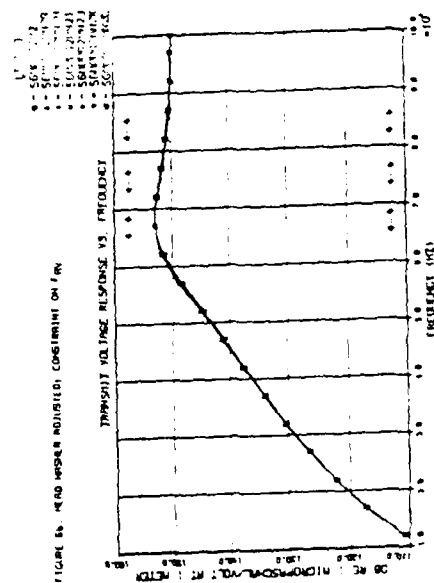
Table 7.1 – Sets of parameter Variations used in first-iteration analysis

PLOT No.	K^T_{33}	s_{33}	s_{33}	SYMBOL	
1	7.5 (%)	7.5 (%)	7.5 (%)	x	
2	5.0	5.0	−5.0	+	
3	2.5	2.5	−2.5		
4	0	0	0	◇	(56 MOD G2M2)
5	−2.5	−2.5	2.5		
6	−5.0	−5.0	5.0		
7	−7.5	−7.5	7.5	⊠	

Table 7.2 – List of plots produced for each case analyzed

PLOT	DESCRIPTION	
1	Input impedance magnitude vs frequency	
2	Input impedance phase vs frequency	
3	Open-circuit receive response vs frequency	
4	Transmit voltage response vs frequency	
5	Transmit current response vs frequency	
6	Source level per field vs frequency	
7	Ceramic in-air admittance vs frequency	
8	Total in-air admittance vs frequency	
9	Tail/head velocity magnitude vs frequency	
10	Tail/head velocity phase vs frequency	
11	Magnitude ZEC11 vs frequency	
12	Magnitude ZIC11 vs frequency	
13	Ratio of head volume velocity modes (w) vs frequency	
14	Source level per volt across ceramic vs frequency	

Planned Validation Experiments

In general, experiments are planned to verify some of the conclusions reached in the single-element theoretical study. However, the hardware is also suitable for extensions planned in the future such as consideration of ring selection procedures.

Experiments have been designed to obtain piezoelectric ceramic parameters via the dumbbell method[6] for one, two, three, and four rings where each ring is measured independently and then the various combinations of rings (two's, three's, four's) are obtained. In each case, whether it be a single ring or more, the dumbbell masses are selected so that the frequency F_m is close to that specified for the PSA. The experiments will be conducted without cement joints.

Parts are available for two complete low-field elements. These components will be modified so that external transformers and inductors may be used for flexibility and so that different ceramic stacks, fiberglass washers, as well as rubber-covered head assemblies may be considered. This effort has been initiated.

Array Modeling

A computerized model is currently being developed to investigate transducer element behavior within the SQS-56 array. To treat radiation interactions between transducers in full generality, the array model includes a dynamic representation of the transducer head using normal modes. Both symmetric (full eight-fold symmetry of the square head) and asymmetric modes are accounted for. Only the symmetric modes are assumed to be driven by the transducer element; asymmetric modes are included as possible scatterers of the radiated field. Inter-modal, inter-element radiation interactions are computed from the Green's function for an infinite rigid baffle. In its current form, the model allows a regular, retangular array on a plane baffle. Modification to a cylindrical baffle, providing a closer approximation to the SQS-56 array, will be accomplished by substituting the appropriate Green's function.

The array model, including flexing heads, interfaces with transducer element models at the stress-rod and ceramic stack annulus. To be consistent with the SEADUCER plane-wave element models, the interface conditions are equality of average velocities and average stresses over the ceramic and stress-rod areas. Element models for various positions within the array need not be identical, thus permitting investigation of array performance with random perturbations in the element construction or ceramic properties. To exercise the model, a rectangular array is defined by number of elements and element separations along each axis. For each element position, a transducer model is created by SEADUCER and reduced to a three-port matrix. Port variables are forces on the stress rod and ceramic stack and either voltage or current at the electrical terminals, depending on drive conditions. (For the SQS-56 array, linkage of the eight elements in a stave to a common drive amplifier will be included in the model at a later time). Applied voltages (currents) corresponding to an intended steering are used as forces on a matrix problem to

41

determine currents (voltages) and stress rod and stack velocities on each element. These can be used either outward, to calculate array source level, receive response level, and beam patterns; or inward to develop detailed analyses of velocities, forces, stresses, strains and electric fields within individual array elements using SEADUCER.

7.4. PLANS

Plans for the FY84 second quarter include the following:

- Add phase transfer graphic outputs for transmit and receive response to augment the existing amplitude plots.

- Begin consideration of ring selection procedures in DAS's.

- Give increased attention to the receive mode in developing DAS's. For example, consider dependent adjustments of ceramic length and head or tail fiberglass washer length.

- Add transmit and receive response and beam pattern outputs to the array predictive capability.

- Obtain more definitive SQS-56 system constratings and requirements on array performance (receive and transmit).

- Begin exercising array predictive model.

- Assess the feasibility of adding a predictive capability for the elastomer on the flexing head.

- Assess feasibility of developing and using a modular power amplifier predictive model.

- Continue in-house experimental hardware development and begin experiments.

- Plan candidate cooperative effort to obtain DAS data as part of the next SQS-56 transducer procurement.

One end product will be a sample specification incorporating a well-understood and carefully controlled DAS. This DAS will be such that a production contractor can still be held responsible for the single-element performance even though most of the components are specified as "build-to-print."

REFERENCES

1. R.W. Timme, "Sonar Transducer Reliability Improvement Program - FY81 Fourth Quarter Progress," NRL Memorandum Report 4615 (1 Oct 1981).

2. C.A. Harper, Handbook of Wiring, Cabling, and Interconnecting for Electronics, McGraw-Hill, New York, pp. 3-45 (1972).

3. J.M. Meek and J.D. Craggs, Electrical Breakdown of Gases, John Wiley & Sons, New York, pp. 533-581 (1978).

4. "Critical Item Production Specification for the Transducer Element of the AN/SQS-56 Sonar," Naval Sea Systems Command, Department of the Navy, Washington, DC (1981).

5. "Inherently Reliable Transducer Design for the SQS-56 Sonar Systems, Volume 1," Naval Ocean Systems Center (report in preparation).

6. "Notes for U.S. Navy Electronics Laboratory Seminar on Transducer Array Analysis and Evaluation" (unpublished) (1965).

DISTRIBUTION LIST

Chief of Naval Research
800 N. Quincy Street
Arlington, VA 22217
ATTN: Code 741, Dr. R.C. Pohanka

Commander
Naval Air Development Center
Warminster, PA 18974
ATTN: Code 3043, R.A. DeChico

Commanding Officer
Naval Coastal Systems Center
Panama City, FL 32407
ATTN: Code 750A, R.L. Cook
       Code 753, R. Lovejoy
       Code 790, D.F. Folds
       Technical Library

Officer-in-Charge
Civil Engineering Laboratory
Naval Construction Battalion Center
Port Hueneme, CA 93043
ATTN: Code L43, J.V. Wilson

Commander
David W. Taylor Naval Ship Research
  and Development Center
Bethesda, MD 20084
ATTN: Technical Library

Commander
Naval Electronics Systems Command
Washington, DC 20360
ATTN: Code 320, Dr. J.A. Sinsky

Commander
Naval Ocean Systems Center
271 Catalina Blvd
San Diego, CA 92152
ATTN: Code 712, D.L. Carson
       Code 712, J. Fransdal
       Code 712, Dr. G. Kinnison
       Code 713, Dr. J. Lockwood
       Code 7123, C.I. Bohman
       Code 7123, J. Wong
       Technical Library

Officer-in-Charge
Naval Sea Systems Command Detachment
Naval Station
Norfolk, VA 23511
ATTN: SEADET6600B10, LT K. Marr

Commanding Officer
Naval Research Laboratory
Washington, DC 20375
ATTN: Code 2628 (32 cys)(12 for DDC)
       Code 5000

Commander
Naval Sea Systems Command
Washington, DC 20362
ATTN: SEA05H, C.C. Taylor
       SEA05N(SSMSO), J. Pratchios
       SEA06H5-21, Ms. D.B. Bagley
       SEA63FP5, S.S. Shimomura
       SEA63R-12, C.C. Walker
       SEA63X, CAPT P.W. Sparks
       SEA63X5, LCDR M. Sherr
       SEA63X5B, R.E. Heaney
       SEA63X5-1, C.A. Clark (3 cys)
       SEA63X5-2, P. Greenhaus
       SEA63X5-3, V. Graves
       SEA63X5-4, T.G. Martin
       SEA63X5-5, B.E. McTaggart

Commander
Naval Surface Weapons Center
White Oak Laboratory
Silver Spring, MD 20910
ATTN: Technical Library

Commanding Officer
Naval Underwater Systems Center
New London Laboratory
New London, CT 06320
ATTN: Code 313, Dr. R. Radlinski
       Code 316, Dr. C.H. Sherman
       Code 316, T.J. Mapes
       Code 3235, R. DeAngelis
       Code 316, C.L. LeBlanc
       Code 316, J.F. Lindberg
       Code 342, T. Suzi
       Code 344, F. Orr
       Code 3222, O. Dickson
       Code 3232, C. Connolly

Naval Underwater Systems Center (con't)
ATTN: Code 3233, J. Gagne
        Code 4111, B. Silver
        Technical Library

Commanding Officer
Naval Underwater Systems Center
Newport Laboratory
Newport, RI 02840
ATTN: Code 38224, Bill Conklin
        Code 382201, Tom Devine

Commanding Officer
Naval Weapons Support Center
Crane, IN 47522
ATTN: Code 705, D. Miley
        Code 70553, D.J. Steele
        Code 70553, K. Niemiller
        Code 70553, T. Peter
        Code 70553, M. Canty
        Code 70555, C. Olds
        Technical Library

Superintendent
Underwater Sound Reference Detachment
Naval Research Laboratory
P.O. Box 8337
Orlando, FL 32856
ATTN: Code 5900
        Code 5905.2 (20 cys)
        Code 5970
        Code 5975 (4 cys)
        Code 5977 (4 cys)
        Code 5978
        Code 5980

Transducer Repair Facility
Mare Island Naval Shipyard
Vallejo, CA 94592
ATTN: Code 270.301, Tow Yee
        Code 967, F. Peglow

Transducer Repair Facility
Pearl Harbor Naval Shipyard
Pearl Harbor, HI 96860
ATTN: Code 191.23, R. Okimoto
        Code 967, P. Pollock

Transducer Repair Facility
Portsmouth Naval Shipyard
Portsmouth, NH 03804
ATTN: Code 270.3, A. Therrien
        Code 967.73, W.W. Lovell
        Code 270.3, J. Mazurek

Ships Parts Control Center
P.O. Box 2020
Mechanicsburg, PA 17055
ATTN: Code 3821, R. Carr

Actran Electroacoustics, Inc.
1012 Maltby Avenue
Orlando, FL 32803
ATTN: C. Sims

Analysis & Technology, Inc.
P.O. Box 769
New London, CT 06320
ATTN: G.E. Sefcik

Ametek Straza
790 Greenfield
El Cajon, CA 92022
ATTN: Head, Transducer Engineering

Battelle Memorial Institute
505 Kind Avenue
Columbus, OH 43201
ATTN: R.J. Dick

Bendix Electrodynamics
15825 Roxford Street
Sylmar, CA 91342
ATTN: J. Martin

Bolt, Beranek & Newman, Inc.
50 Moulton Street
Cambridge, MA 02138
ATTN: N. Higbie
        Dr. S. Africk
        Dr. N.C. Martin

Dyna-Empire, Inc.
1075 Stewart Avenue
Garden City, LI, NY 11530
ATTN: A. Backran
        E. Freidel

EDO Corporation
14-04 111th Street
College Point, NY 11356
ATTN: S. Schildkraut

Edo Western Corporation
2645 South 300 West
Salt Lake City, UT 84115
ATTN: D. Bonnema
        G.L. Snow

General Electric
P.O. Box 4840
Syracuse, NY 13221
ATTN: J. Dietz

General Instrument Corporation
Government Systems Division
33 Southwest Industrial Park
Westwood, MA 02090
ATTN: D. White
       A. Poturnicki

General Instrument Co.
600 W. John Street
Hicksville, NY 11802
ATTN: E. Klosko, Reliability Mgr

Gould, Inc.
Ocean Systems Division
18901 Euclid Avenue
Cleveland, OH 44117
ATTN: M.R. Collins
       S. Thompson
       A. Irons
       J. Gray

Hazeltine Corporation
115 Baystate Drive
Braintree, MA 02184
ATTN: H.M. Lamb

Honeywell, Inc.
Marine Systems Center
5303 Shilshole Avenue, NW
Seattle, WA 98107
ATTN: C. Sheets
       O.L. Ackervold
       Technical Information Center

Honeywell, Inc.
Honeywell Ceramics Center
5121 Winnetka Avenue N
New Hope, MN 55428
ATTN: D.W. Bacso

International Transducer Corporation
640 McCloskey Place
Goleta, CA 93017
ATTN: G.E. Liddiard
       F. Dutton

Magnavox Co.
1313 Production Road
Ft Wayne, IN 46808
ATTN: D. Kulpa

MAR, Inc.
1335 Rockville Pike
Rockville, MD 20852
ATTN: Dr. W. Cramer

Potomac Research
1600 N. Beauregard Street
Alexandria, VA 22311
ATTN: P.B. Watson

Raytheon Co.
Submarine Signal Division
P.O. Box 360
Portsmouth, RI 02871
ATTN: N. Serotta, K_{33} Transducer
              Program Mgr
           D. Ricketts, Consultant,
              Design Engr Laboratory
           M. Relyea, Mgr, Transducer
              Dept

Sperry Rand Corporation
Sperry Gyroscope Division
Marcus Avenue
Great Neck, NY 11020
ATTN: M/S D-18, G. Rand

Texas Research Institute, Inc.
5902 West Bee Caves Road
Auston, TX 78746
ATTN: Dr. J.S. Thornton (2 cys)

TRACOR, Inc.
Systems Technology Division
1601 Research Blvd
Rockville, MD 20850
ATTN: P.D. Flannery
       J. Guarnieri
       J.W. McClung
       D. Abraham

TRACOR, Inc.
19 Thames Street
Groton, CT 06340
ATTN: G.M. Ross

TRW, Inc.
One Space Park
Redondo Beach, CA 90278
ATTN: A. Samsonov, Head Engr
            Applications Section

TRW, Inc.
7600 Colshire Drive
McLean, VA 22102
ATTN: J. Mahler

Underwater Systems Acoustics
2627 Burgener Blvd
San Diego, CA 92210
ATTN: Dr. G.E. Martin

Westinghouse Electric Corporation
P.O. Box 1488
Annapolis, MD 21404
ATTN: M/S 9R40, C.R. Wilson

W.L. Hufferd & Associates
Consulting Engineers
2826 Devereaux Way
Salt Lake City, UT 84109

Wyle Labs
P.O. Box 1008
Huntsville, AL 35807
ATTN: D. Moore

Georgia Institute of Technology
Electromagnetic Capability Division
   Electronics & Computer Systems
Atlanta, GA 30332
ATTN: Dr. H.W. Denny

University of Washington
Applied Physics Laboratory
1013 NE 40th
Seattle, WA 98105
ATTN: Dr. C.J. Sandwith

Applied Research Laboratory
University of Texas at Austin
P.O. Box 8029
Austin, TX 78712
ATTN: Dr. D. Baker

Director of Naval Weapons Design
Department of Defense (Navy)
Campbell Park 1 (Room 6-18)
Canberra, A.C.T. 2600 Australia

Mulloka Project Director - Navy
Department of Defense (Navy)
Campbell Park 2 (Room 1-24)
Canberra, A.C.T. 2600 Australia
ATTN: CDR P. Hart

Director of Fleet Maintenance (WU)
Department of Defense (Navy)
Campbell Park 1 (Room 3-11)
Canberra, A.C.T. 2600 Australia

Admiralty Marine Technology
   Establishment
Holton Heath
Poole, Dorsett, England
ATTN: Mr. B.H. Nicholls

AE/USE-AEL
Building 26
T.S.A.S.
Defense Research Centre
Salisbury, S.A. 5108 Australia

EMI (Australia) PTY Ltd
P.O. Box 161
Elizabeth, S.A. Australia
ATTN: J. Nankivell

Materials Research Laboratory
P.O. Box 50
Ascot Vale, Victoria, Australia
ATTN: Dr. D. Oldfield

Plessey Company Ltd
Plessey Marine Research Unit
Templecombe, Somerset, England
ATTN: W. Craster

Plessey (Australia) PTY Ltd
Faraday Park Road
Meadowbank, N.S.W. 2114 Australia
ATTN: G. Tulloch

Defense Equipment Center
British Defense Staff
British Embassy
Washington, DC 20008
ATTN: Derek Palmer, Materials Officer

DB Instrumentation, Ltd
111 Victoria Road
Aldershot, Hants, England
ATTN: L.W. Lipscombe, Director

Robert Gordon's Institute of Technology
School of Physics
Aberdeen ABQ IFR
Scotland
ATTN: Dr. R. Hill